RECENT RESULTS OF H-MODE CONFINEMENT STUDY IN JT-60U (APRIL-SEPTEMBER, 1995)

November 1995

JT-60U H-mode Study Group

Recent Results of H-mode Confinement Study in JT-60U (April-September, 1995)

JT-60U H-mode Study Group

Department of Fusion Plasma Research
Naka Fusion Research Establishment
Japan Atomic Energy Research Institute
Naka-machi, Naka-gun, Ibaraki-ken

Improvement in the performance of energy confinement is one of the most important issues to realize thermonuclear fusion reactors. The H-mode is one of excellent improved confinement modes. From the view point of steady-state operation, the ELMy H-mode is considered to be a principal operation mode in ITER. For the engineering design of the ITER, there still remain issues to be clarified on the H-mode characteristics. These issues are required to be studied on the present tokamaks as ITER physics research needs.

In order to satisfy the above request, experiments of the H-mode confinement have been carried out on JT-60U. Recent results of H-mode confinement stydy in JT-60U during April to September, 1995 are summarized in the present report. The scaling of high T_i H-mode confinement is described in section 2. The time behaviour of transport properties are shown in sections 3 and 4. Result of the non-dimensional transport experiment is presented in section 5. The H-mode transition is investigated in sections 6, 7, 8 and 9; threshold power scaling, parametric study on edge local quantities, effect of edge neutrals, and H-L back transition. The onset condition of ELMs is studied in section 10.

ＪＴ−６０ＵにおけるＨモード閉じ込め研究の最近の成果（1995年4月−9月）

日本原子力研究所那珂研究所炉心プラズマ研究部
ＪＴ−６０Ｕ　Ｈモード研究グループ

　　熱核融合炉実験のためにはエネルギー閉じ込め性能の改善が最重要課題の一つである。優れた改善モードの一つとしてＨモードがある。定常運転の観点から，ＩＴＥＲでは主要な運転モードとしてＥＬＭｙ　Ｈモードが考えられている。ＩＴＥＲの工学設計において，Ｈモードの特性に関し未だ解明されていない問題点が残っている。これらの問題点に対し，ＩＴＥＲ物理Ｒ＆Ｄとして研究を進めることが要求されている。

　　この要求に応えるために，ＪＴ−６０ＵにおいてＨモード閉じ込め研究が行われてきた。この報告書は，1995年4月から9月の間に行われたＨモード閉じ込め研究の最近の成果をまとめたものである。第2節には高イオン温度Ｈモードの閉じ込めの比例則が記述されている。第3節と4節には，輸送特性の時間的挙動が示されている。第5節には，無次元輸送実験の結果が表されている。第6，7，8，9節では，Ｈモード遷移に関する研究が行われた：パワー閾値の比例則，周辺プラズマ物理量のパラメータ依存性，中性粒子の影響，Ｈ−Ｌバック遷移について調べられている。第10節にはＥＬＭの発生条件が示されている。

那珂研究所：〒311-01　茨城県那珂郡那珂町向山801-1

Contents

目　　次

1. Introduction

Improvement in the performance of energy confinement is one of the most important issues to realize thermonuclear fusion reactors. On the basis of the L-mode confinement performance, a tokamak reactor will require a large value of AXI_p of more than 100 MA, where A is the aspect ratio and I_p is the plasma current. This value is too large for the economic and engineering view points. Therefore the improved confinement should be realized in the fusion plasmas.

Various kinds of improved confinement modes have been found out and developed on many tokamaks in the world. The H-mode is one of excellent improved confinement modes. This mode has a characteristic of the edge transport barrier. The feature of improved core confinement is sometimes combined with that of H-mode, and higher performance of the energy confinement has been attained through this combination.

From the view point of steady-state operation, ELMs (Edge Localized Modes) are useful for the particle control, although the energy confinement performance is slightly degraded by them. The ELMy H-mode is considered to be a principal operation mode in ITER.

For the engineering design of the ITER, there still remain issues to be clarified on the H-mode characteristics, such as energy confinement time scaling, H-mode power threshold scaling, non-dimensional transport, ELM model and so on. These issues are required to be studied on the present tokamaks as ITER physics research needs [1.1].

In order to satisfy the above request, experiments of the H-mode confinement have been carried out on JT-60U. Recent results of H-mode confinement study in JT-60U during April to September, 1995 are summarized in the present report. The scaling of high T_i H-mode confinement is described in section 2. The time behaviour of transport properties are shown in sections 3 and 4. Result of the non-dimensional transport experiment is presented in section 5. The H-mode transition is investigated in sections 6, 7, 8 and 9; threshold power scaling, parametric study on edge local quantities, effect of edge neutrals, and H-L back transition. The onset condition of ELMs is studied in section 10.

The authorship for each study lies on the authors of each section, and there is no special authorship for the whole report.

References
[1.1]   ITER Physics Committee, ITER Physics Committee Meeting, Naka, 1994 .

2. Scaling of High T_i H-mode Confinement in JT-60U

Tomonori TAKIZUKA, Mitsuru KIKUCHI, Hiroshi SHIRAI

2.1 Introduction

In order to make a tokamak fusion reactor being compact, improvement in the energy confinement from L-mode state is indispensable. At the present time, the physical mechanisms of the energy transport and of its improvement are not clarified, and the confinement performance in future tokamak reactors is estimated by using scaling laws empirically obtained from the existing confinement database. The energy confinement time τ_E of L-mode plasmas can be predicted by a scaling law called ITER89 power law scaling [2.1];

$$\tau_E^{ITER89P} = 0.038 \ M^{0.5} \ I_p^{0.85} \ B_t^{0.2} \ n_e^{0.1} \ R^{1.2} \ a^{0.3} \ \kappa^{0.5} / P_{net}^{0.5} . \tag{2.1}$$

The units in the scaling expression are following; confinement time τ is in s, plasma current I_p in MA, toroidal field B_t in T, line averaged density n_e in 10^{19} m^{-3}, major radius R in m, minor radius a in m, and net power P_{net} is in MW. The ion mass number is denoted by M and the ellipticity by κ.

Several kinds of improved confinement modes have been found in tokamak experiments, such as H-mode, Supershot, high β_p mode, VH-mode and so on. Measure of the improvement in the energy confinement is usually based on the above scaling, i.e., H-factor is defined as $H = \tau_E / \tau_E^{ITER89P}$. The values of H-factor in improved confinement plasmas are not constant at all. As for the H-mode, one sees from the ITER H-mode confinement database that H-factor increases with the plasma size. A resultant scaling expression for ELM-free H-mode is given by [2.2]

$$\tau_E^{ELM-free} = 0.045 \ M^{0.43} \ I_p^{0.87} \ B_t^{0.45} \ n_e^{0.03} \ R^{1.86} \ a^{-0.02} \ \kappa^{0.53} / P_{net}^{0.55} . \tag{2.2}$$

For the design of tokamak reactors, the confinement performance of thermal energy is more important than that of total energy which includes the high energy α particle component. A scaling of the thermal energy confinement time for ELM-free H-mode is also given by [2.2]

$$\tau_{th}^{ELM-free} = 0.036 \ M^{0.41} \ I_p^{1.06} \ B_t^{0.32} \ n_e^{0.17} \ R^{1.9} \ a^{-0.11} \ \kappa^{0.66} / P_{net}^{0.67} . \tag{2.3}$$

In the present paper, we compare the results of ELM-free H-mode confinement in JT-60U with above scaling laws. The data used in this paper are collected from the shots between E16098 and E16265, which were discharged in September 1992. The plasma shapes were almost the same in the data; $R \approx 3.2$ m, $a \approx 0.85$ m, and $\kappa \approx 1.65$. This database was used to show, in Fig. 6 of Ref. [2.3], the relation between H-factor and the effective safety factor q_{eff}.

In this database, the net power was evaluated by considering effects of shinethrough loss of beam neutrals, ripple loss of beam ions [2.4], time derivative of stored energy etc. We also investigate the effect of high ion temperature ($T_i/T_e > 1$) on the improvement in energy confinement, and a scaling expression for H-mode confinement including its effect is shown. Generalized H-mode database including hot ion mode and scaling laws for them are required as ITER physics research needs [2.5]. The present paper is the first and preliminary step for this requirement.

2.2 Comparison with scaling laws

Figure 2.1 shows the comparison of τ_E of H-mode plasmas in JT-60U with $\tau_E^{ITER89P}$. In this subsection, the data of low H-factor (H < 1.1) are omitted. The average of H-factor for these data is about 1.8 excluding data of low q_{eff} ($q_{eff} < 3.3$), which have low H-factor [2.3] and are plotted by closed circles. The horizontal axis, therefore, is chosen as $1.8 \times \tau_E^{ITER89P}$. The scattering of data points from the line of proportion is rather large. The standard deviation σ_y ($\sigma_y^2 = N^{-1} \Sigma(\tau/\tau^{fit} - 1)^2$) is about 0.15 excluding data of low q_{eff}. This value is as large as the standard deviation of variation in τ; $\sigma_x = 0.16$ ($\sigma_x^2 = N^{-1} \Sigma(\tau/<\tau> - 1)^2$, where N is the number of data points and $<\tau> = N^{-1} \Sigma \tau$.

Next we compare the data with H-mode scaling laws in Fig. 2.2 (τ_E vs $\tau_E^{ELM-free}$). The H-factor predicted by Eq. (2.2), $H_E^* = \tau_E^{ELM-free}/\tau_E^{ITER89P}$, is roughly given as $H_E^* \approx$ $1.1 \, B_t^{0.25} R^{0.66} a^{-0.32}/P_{net}^{0.05}$. For the typical parameters of JT-60U H-mode plasmas, values of H_E^* are from 3 to 3.5. These values are too large compared with experimental data of JT-60U as is clearly seen in Fig. 2.2. Even when we compare the data with the thermal confinement scaling given by Eq. (2.3), we find that majority of predicted values exceed experimental data. The H-factor predicted by Eq. (2.3), $H_{th}^* = \tau_{th}^{ELM-free}/\tau_E^{ITER89P}$, is given as $H_{th}^* \approx 0.9 \, I_p^{0.21} B_t^{0.11} R^{0.7} a^{-0.41} \kappa^{0.16}/P_{net}^{0.17}$. For the typical parameters, values of H_{th}^* are from 2 to 2.5.

It is necessary to establish a new scaling which will be able to fit the H-mode confinement data of JT-60U as well as the data of ITER H-mode confinement database. It should be noted that JT-60U data are not included in the ITER H-mode confinement database at present, because JT-60U data with high T_i nature ($T_i/T_e > 1$) are out of the standard data with nearly equal temperatures ($T_i/T_e \approx 1$).

2.3 Effect of high T_i on the improvement

To obtain high H-factor in JT-60U plasmas, the high T_i condition ($T_i/T_e > 1$) has been inevitable (a necessary condition) so far. The high value of T_i/T_e, however, has been considered not a sufficient condition. Figure 2.3 shows the relation between the H-factor and the temperature ratio at the plasma center, T_{i0}/T_{e0}. As is mentioned above, high H-factor is

realized only for high T_{i0}/T_{e0}. The data with Bt $\approx$ 4.2 T / Ip $\approx$ 2.7 MA (qeff $\approx$ 4.2) are selected as shown in Fig. 2.4, where the correlation between H-factor and T_{i0}/T_{e0} seems very weak. We find, however, this scattering is caused by the variation of n_e value. We introduce an improvement rate defined as $(H - 1)/(T_{i0}/T_{e0} - 1)$. Figure 2.5 demonstrates the clear dependence of the improvement rate on the line averaged density; $(H - 1)/(T_{i0}/T_{e0} - 1)$ is almost proportional to $n_e^{1.5}$. The H-factor increases not only with T_{i0}/T_{e0} but also with n_e. The I_p and B_t dependencies of H-factor are also investigated in the range, 1.5 MA < I_p < 3.5 MA and 3.0 T < B_t < 4.2 T (3.1 < qeff < 6.3). Figure 2.6 shows $(H - 1)/(T_{i0}/T_{e0} - 1)$ $n_e^{1.5}$ vs I_p for qeff > 3.3, where open circles represent the data of $B_t \approx$ 4.2T and closed squares represent the data of $B_t \approx$ 3.1T. The values of $(H - 1)/(T_{i0}/T_{e0} - 1)$ $n_e^{1.5}$ is inversely proportional to I_p^2 while the B_t dependence of $(H - 1)/(T_{i0}/T_{e0} - 1)$ $n_e^{1.5}$ is weak as shown in Fig. 2.7, where $(H - 1)$ $I_p^2/(T_{i0}/T_{e0} - 1)$ $n_e^{1.5}$ vs B_t is plotted.

Finaly we obtain a following fitting formula;

$$(H^{fit} - 1)/(T_{i0}/T_{e0} - 1) = C \, n_e^{1.5}/I_p^2 \qquad \text{with } C = 1 . \tag{2.4}$$

Figure 2.8 shows τ_E vs τ_E^{fit}, where $\tau_E^{fit} = H^{fit} \times \tau_E^{ITER89P}$. The standard deviation σ_y is reduced to 0.098 excluding data of low qeff, and the clear correlation is seen. Note that the data of low H-factor are not excluded in this subsection unlike subsection 2.2.

When H-factor become large, Eq. (2.4) simply gives that τ_E is inversely proportional to I_p because H ~ I_p^{-2} and $\tau_E^{ITER89P}$ ~ I_p. In a highly improved plasma with large H-factor, however, there exists the strong correlation between parameters, such as $(T_{i0}/T_{e0} -1)$ ~ B_t , n_e ~ $I_p^{0.5}$ etc. Therefore the obtainable τ_E value at the same P_{net} is not inversely proportional to I_p but is almost independent of I_p. On the other hand it increases with higher B_t.

2.4 Summary

We have compared the confinement data of ELM-free high T_i H-mode in JT-60U with an L-mode scaling law (ITER-89 power law) and ELM-free H-mode scaling laws. The average of H-factor for the present data is about 1.8, which is much smaller than that expected from the ELM-free H-mode scaling (H $\approx$ 3). The scattering from a fitting line, τ_E = 1.8 $\times$ $\tau_E^{ITER89P}$, is rather large. In order to clarify the effect of high T_i, we have carried out a preliminary analysis of the data, and found for the first time that values of H-factor are fitted well by a formula, $H^{fit} = 1+(T_{i0}/T_{e0} - 1) \, n_e^{1.5}/I_p^2$

The database used here are limitted one. In order to check the validity of the present formula and to refine it, replenishment of the database will be progressed in near future.

Acknowledgment

References

[2.1] P.N. Yushmanov, T. Takizuka, K.S. Riedel et al., Nucl. Fusion 30 (1990) 1999.

[2.2] ITER H Mode Database Working Group, Nucl. Fusion 34 (1994) 131.

[2.3] M. Sato, M. Kikuchi, T. Fukuda et al., 15th Int. Conf. on Plasma Physics and Contr. Nucl. Fusion Research, Seville, 1994, IAEA-CN-60/A-2-II-4

[2.4] A.A.E. van Blokland et al., Plasma Phys. Contr. Fusion 36 (1994) 925.

[2.5] ITER Physics Committee, ITER Physics Committee Meeting, Naka, 1994 .
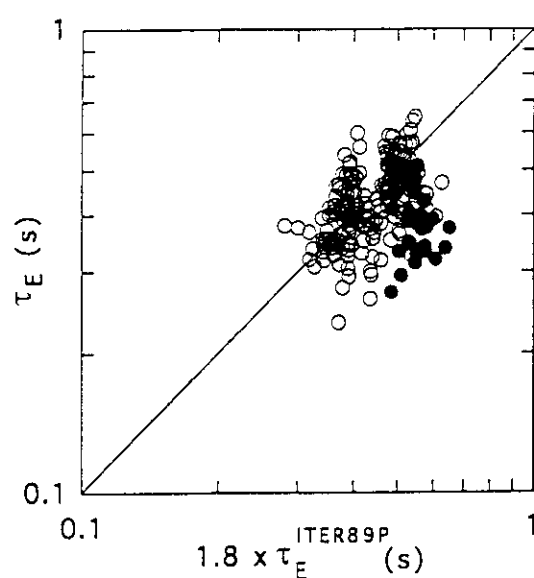
Fig. 2.1 Comparison of energy confinement ime τ_E of ELM-free high T_i H-mode in JT-60U with $1.8 \times \tau_E^{ITER89P}$. Closed circles represent the data of $q_{eff} < 3.3$.
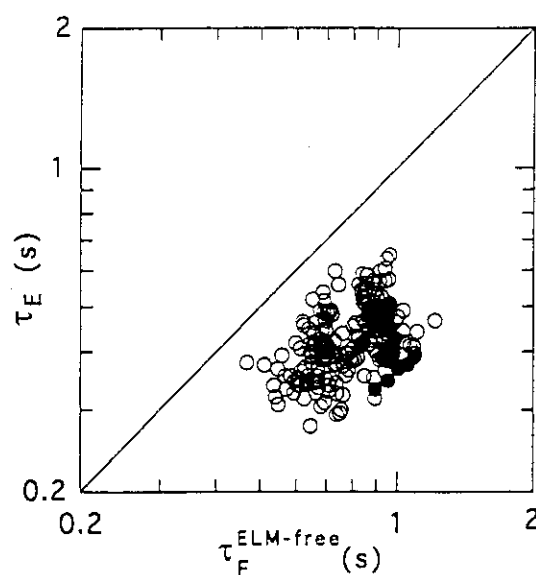
Fig. 2.2 Comparison of τ_E with $\tau_E^{ELM-free}$. Closed circles represent the data of $q_{eff} < 3.3$.
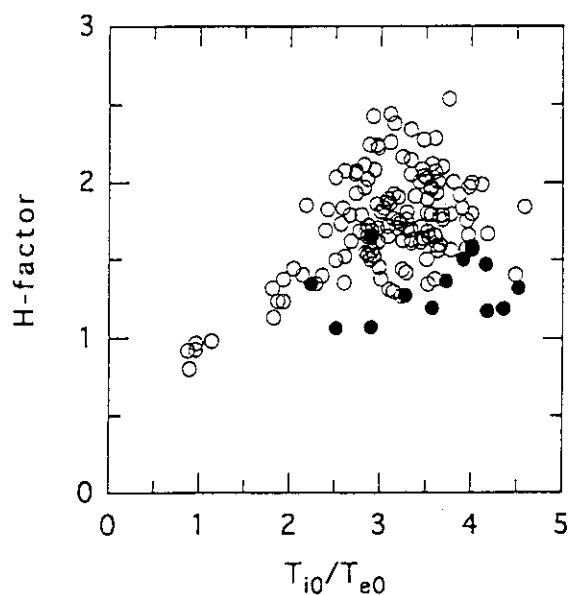
Fig. 2.3 Relation between H-factor and temperature ratio at the plasma center, T_{i0}/T_{e0}. Closed circles represent the data of $q_{eff} < 3.3$.
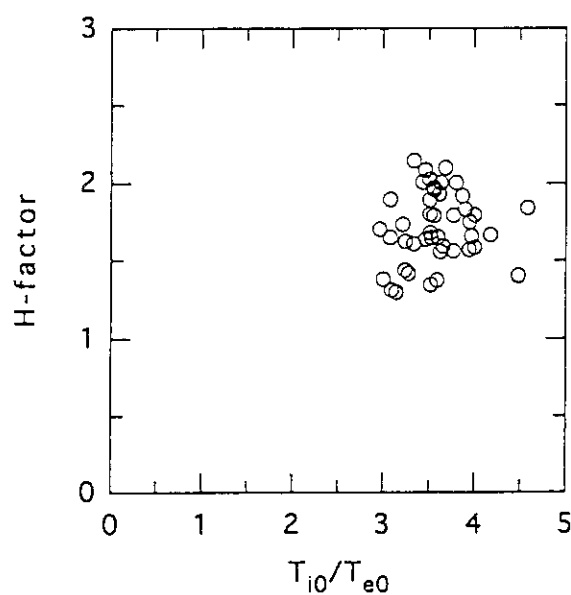
Fig. 2.4 Relation between H-factor and T_{i0}/T_{e0} for Bt $\approx$ 4.2 T / Ip $\approx$ 2.7 MA (qeff $\approx$ 4.2).
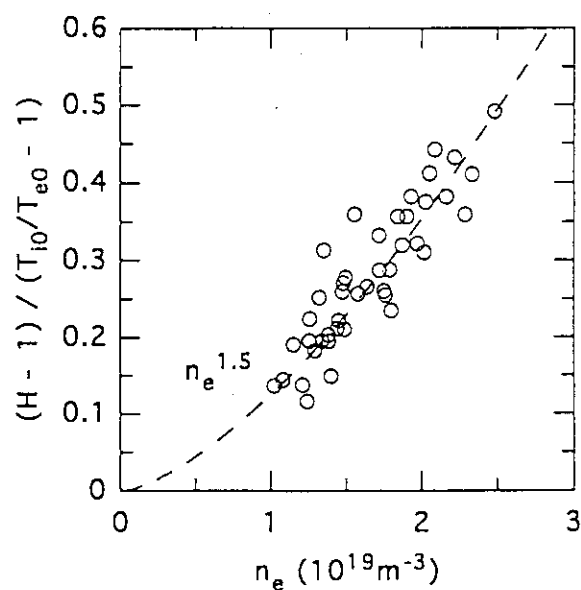
Fig. 2.5 Dependence of improvement rate (H - 1)/(T_{i0}/T_{e0} - 1) on n_e for Bt $\approx$ 4.2 T / Ip $\approx$ 2.7 MA (qeff $\approx$ 4.2). The rate is almost proportional to $n_e^{1.5}$.
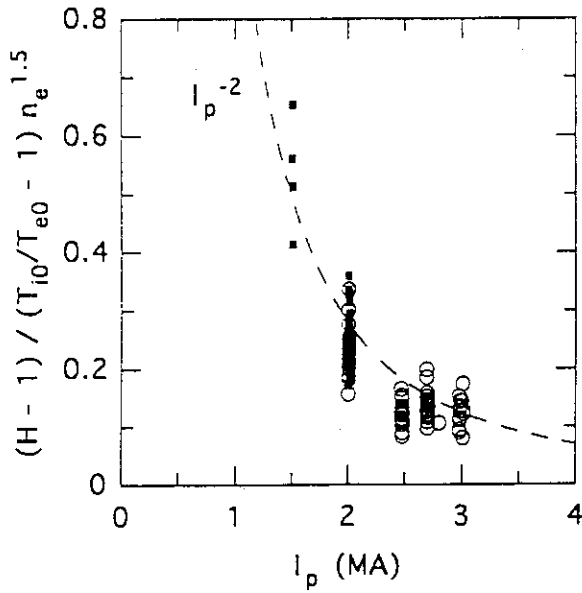
Fig. 2.6 Dependence of improvement rate divided by $n_e^{1.5}$, $(H - 1)/$ $(T_{i0}/T_{e0} - 1)$ $n_e^{1.5}$, on I_p for $B_t \approx$ 4.2 T (open circles) and $B_t \approx 3.1$ T (closed squares). The rate is almost proportional to I_p^{-2}.
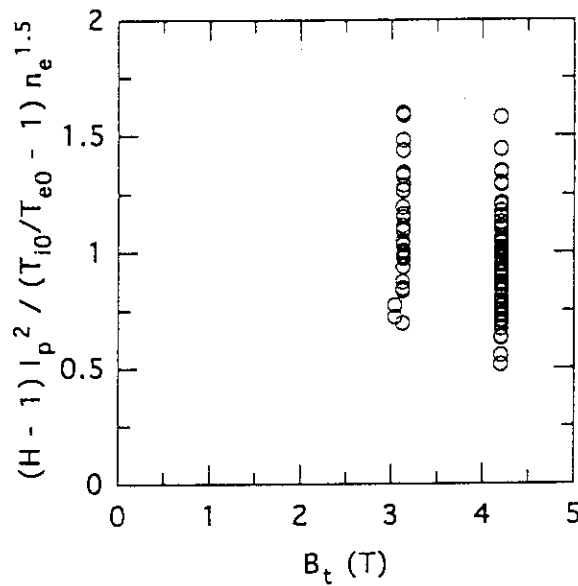
Fig. 2.7 Improvement rate multiplied by $I_p^2 / n_e^{1.5}$, $(H - 1)$ $I_p^2/$ $(T_{i0}/T_{e0} - 1)$ $n_e^{1.5}$, vs B_t.
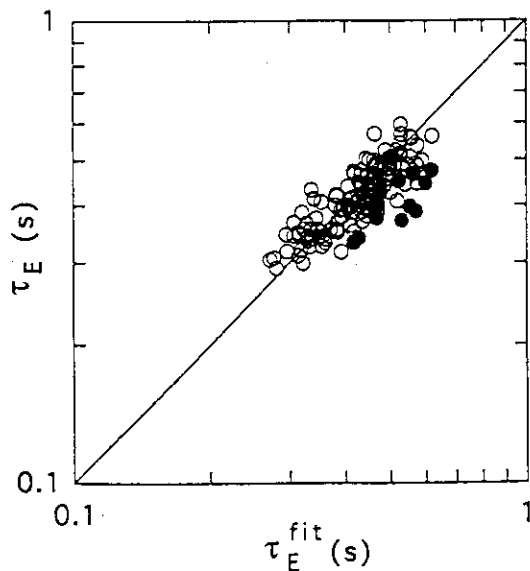
Fig. 2.8 Comparison of τ_E with τ_E^{fit}. Fitting formula is given as $\tau_E^{fit} = H^{fit} \times \tau_E^{ITER89P}$ with $(H^{fit} - 1)/(T_{i0}/T_{e0} - 1) =$ $n_e^{1.5}/I_p^2$. Closed circles represent to data of $q_{eff} < 3.3$.

3. Time Behaviour of Heat Diffusivity during L-H-L Transitions in JT-60U

Tomonori TAKIZUKA, Sergei V. NEUDATCHIN*, Hiroshi SHIRAI, Nobuaki ISEI,

Yutaka KAMADA, Yoshihiko KOIDE, Masayasu SATO, Masafumi AZUMI

*Nuclear Fusion Institute, Russian Research Center, "Kurchatov Institute", Moscow, Russia

3.1 Introduction

An understanding of the time evolution of local transport coefficients during a transition between various confinement regimes is important to clarify the physical mechanism responsible for the anomalous transport observed in tokamak plasmas.

In relation to L-H-L transitions on JET, the time evolutions of electron temperature T_e, ion temperature T_i, electron heat diffusivity χ_e, and ion heat diffusivity χ_i have been analyzed and reported previously [3.1,3.2]. The simultaneous T_e response was clearly seen during L-H-L transitions in the plasma region, $0.2 < r/a < 1$. To describe this event, we apply a simple heat diffusion equation with the change in χ_e after the transition. It was shown that this χ_e jump, $\delta\chi_e$, occurs across almost all plasma volume on a millisecond time scale. Let us remind that in the "traditional picture" the L-H or H-L transition occurs near the plasma surface, and the confinement improvement in plasma interior then evolves on a time scale of the order of the energy confinement time τ_E [3.3]. It was not obvious up today whether these diffusivity jumps across almost all plasma volume are the peculiar feature of JET or not.

In order to answer above questions, we have investigated the time evolution of χ_e and χ_i during L-H-L transitions on JT-60U [3.4,3.5]. The present paper is a review of our investigations.

3.2 Analyses of $\delta\chi$ during transitions

We analyze the jumps of χ, $\delta\chi$, during L-H-L transitions on JT-60U mainly for high field pulses ($B_t \approx 4$ T). Typical shape parameters are $R \approx 3.2$ m, $a \approx 1.05$ m (volume-averaged one), $\kappa \approx 1.6$, $\delta < 0.1$, and $V \approx 70$ m^3. We restrict the analyses here for the cases of L-H-L transitions, after the improved confinement with high H-factor (ratio of τ_E to $\tau_E^{ITER89P}$) is well developed, because the change in the global parameters is clearly seen during these transitions.

The time evolution of electron temperature profile, $T_e(\rho, t)$, is measured by ECE grating polychromator and that of ion temperature profile, $T_i(\rho, t)$, is measured by charge-exchange recombination spectroscopy. The normalized radial position, $\rho = r/a$, are labeled in the following figures of time evolutions of T_e and T_i.

Figure 3.1 shows the time evolution of plasma parameters in a high T_i H-mode pulse E17058 (3.5 MA / 4.2 T), where a clear H-L transition occurred at t = 8.38 s. In the figure, the plasma current I_p, the line integrated electron density n_eL (length L is about 2.5 m), the stored energy measured by diamagnetic loop W, the injected neutral beam power P_{NB}, and the Hα intensity from the divertor region Hαdiv are shown. The growth of W was interrupted by the H-L transition and Hαdiv abruptly increased. The value of τ_E before the time A is about 380 ms (H $\approx$ 1.5) and $\tau_E \approx$ 190 ms (H $\approx$ 1.0) after A. Figure 3.2 shows the time evolutions of $T_e(\rho, t)$ and $T_i(\rho, t)$. Sawtooth crash occurs about 50 ms after the transition A. The beginning of the decay of ECE signals over the region $0.43 < \rho < 0.83$ and the jump of Hα occur simultaneously (about 10 ms uncertainties). $T_i(\rho, t)$ behaves similarly to $T_e(\rho, t)$.

It is natural for us to explain the sudden change in T_e at a transition caused by sudden variation of the electron heat flux. As described in Refs. [3.1,3.2] we apply a simple heat diffusion equation with the change in χ_e across almost all plasma volume after the transition. The value of χ_e jump, $\delta\chi_e$, can be estimated easily from $T_e(\rho, t)$. Values of $\delta\chi_e$ after the above H-L transition are about 0.65 m²/s and 0.85 m²/s at $\rho \approx$ 0.61 and 0.71, respectively. The value of $\delta\chi_i$ is about 0.55 m²/s at $\rho \approx$ 0.56, which is almost the same as that of $\delta\chi_e$.

For the central region, $\rho < 0.36$, however, the time delay of T_e response is seen as was observed in JET [3.1,3.2]. This result shows that the heat pulse propagation (HPP) may play important role near the center or that the improvement and degradation of transport may propagate from the mid region to the center with the propagation speed of about 10 m/s.

The L-H and H-L transitions in a low-Ip pulse 17038 (2 MA / 4.2 T) are studied. Figure 3.3 shows evolutions of $T_e(\rho, t)$ and $T_i(\rho, t)$. Waveforms of W, P_{NB} and Hαdiv are also shown to compare the time response of T_e and T_i . During short ELM-free H-mode phases (A-B and C-D) values of τ_E are about 330 ms (H $\approx$ 1.8), while during high-T_i L-mode phases (before A, B-C, and after D) $\tau_E \approx$ 190 ms (H $\approx$ 1.3). The simultaneous response of T_e and T_i over $0.3 < \rho < 0.8$ is clearly seen in Figs. 3.4 and 3.5. The value of $\delta\chi_e$ after the L-H transition C is about -0.65 m²/s at $\rho \approx$ 0.63, of which absolute value is almost the same as those at $\rho \approx$ 0.6 for higher-Ip pulses. On the other hand, values of $\delta\chi_i$ after C are about -0.64 m²/s and -0.93 m²/s at $\rho \approx$ 0.55 and 0.63, respectively. These values are almost the same as or a little higher than those for high-Ip pulses.

Values of $\delta\chi$ analyzed for various pulses are summarized in Table 3.1.

3.3 Discussion

We examine whether obtained values of $\delta\chi$ are consistent with the change of τ_E during transitions. Though the value of τ_E was calculated not from the thermal stored energy but from the total stored energy including fast ion component, the following approximate relation is used for the comparison between $|\delta\chi|$ and the change of τ_E; $\tau_E \approx a^2 / 4\chi_{\rho \approx 0.6}$ and $|\delta\chi_{\rho \approx 0.6}| \approx$

$(a^2/4) \{ \tau_E(L)^{-1} - \tau_E(H)^{-1} \}$. Here we consider cases of $\delta\chi_e \approx \delta\chi_i$ and the smooth radial variation of $\delta\chi$. Typical values of $\tau_E(L)$ and $\tau_E(H)$ in plasmas of $a \approx 1.05$ m are about 0.2 s and 0.4 s, respectively, and the value of $|\delta\chi_{\rho \approx 0.6}|$ is about 0.6 m²/s. These values roughly satisfies the above relation. This result supports the validity of the present model in which χ jumps simultaneously over the wide plasma region during a transition.

The behaviour of χ_i for a low field pulse 17298 with 1.5 MA / 2.5 T is analyzed for comparison. The polychromator data are not available to use for low field pulses, $B_t < 3.5$ T. Clear L-H-L transitions were repeated in a shot E17298. High values of $\delta\chi_i$ are obtained as listed in Table 3.1. These values are about three times larger than those for high field pulses on JT-60U, but similar to those of JET data [3.1,3.2]. If we combine JT-60U data and JET data together, we suppose that the dependence of $\delta\chi_i$ is negative on B_t like $1/B_t$, while the dependence of $\delta\chi_e$ is weak on B_t. The tendency of the negative dependence on I_p is also seen for $\delta\chi_i$. The increase of χ_i^{PB} with decrease of I_p in JT-60U L-mode plasmas was found from the power balance analysis [3.6]. The weak I_p dependence of χ_e^{PB} was also reported in Ref. [3.6]. These dependencies on I_p are in qualitative agreement with each other.

3.4 Conclusion

We have analyzed L-H-L transitions mainly for high field pulses in JT-60U [3.4,3.5]. The simultaneous T_e response (with uncertainty of 10 ms) has been clearly observed during L-H-L transitions over $0.2 < \rho < 0.9$ in JT-60U plasmas similarly in JET [3.1,3.2]. This evolution of $T_e(\rho, t)$ is difficult to be explained as the result of HPP from the periphery, but is reasonable to be described as the result of the fast χ_e jump (reduction at L-H transitions and increment at H-L transitions) over $0.2 < \rho < 0.9$. The simultaneous T_i response (with uncertainty of 20 ms) were also observed similarly to the T_e response. The fast variation of χ (at least 20-40 times less than τ_E) inside almost all plasma volume is a new finding of the L-H-L transitions in JT-60U. The T_e response in the central region ($\rho \sim 0.3$) often delays, compared with that in the outer region ($\rho \sim 0.5$) seen, and the role of HPP could be important similarly to JET results [3.1,3.2]. Values of χ_e jump, $\delta\chi_e$, were obtained for $0.5 < \rho < 0.7$, whose absolute values were 0.6 m²/s $< |\delta\chi_e| < 0.9$ m²/s. They usually increase with radius. Values of $\delta\chi_i$ were also obtained for $0.4 < \rho < 0.7$. Their absolute values, $|\delta\chi_e|$ and $|\delta\chi_i|$, usually increase with radius. In high I_p pulses ($I_p > 3$ MA / $B_t = 4.2$ T), values of $|\delta\chi_i| \approx 0.5$ m²/s are almost the same as or a little smaller than those of $|\delta\chi_e|$, while in a low I_p pulse (2 MA / 4.2 T), values of 0.6 m²/s $< |\delta\chi_i| < 1$ m²/s are almost the same or a little larger than $|\delta\chi_e|$. In a low field pulse (1.5 MA / 2.5 T), values of $|\delta\chi_i|$ are rather large as 2 m²/s at $\rho \approx 0.60$.

Values of $\delta\chi$ are consistent with the change of τ_E during transitions. The dependence of $\delta\chi_i$ is negative on B_t or I_p like $1/B_t$ or $1/I_p$, while the B_t or I_p dependence of $\delta\chi_e$ is weak.

These I_p dependencies agree qualitatively with the result of power balance analysis for JT-60U L-mode plasmas [3.6].

References

[3.1] J.G. Cordey, D.G. Muir, S.V. Neudatchin et al., Plasma Phys. and Contr. Fusion 36 Suppl. (1994) A267.

[3.2] J.G. Cordey, D.G. Muir, S. V. Neudatchin et al., Nucl. Fusion 35 (1995) 101.

[3.3] R.J. Groebner, Phys. Fluids B 5 (1993) 2343.

[3.4] S.V. Neudatchin, H. Shirai, T. Takizuka et al., "The Time Behaviour of the Heat Conductivity during L-H-L Transitions in JT-60U", 22nd EPS Conf. on Contr. Fusion and Plasma Phys., Bournemouth, 3-7 July 1995.

[3.5] S.V. Neudatchin, T. Takizuka, H. Shirai et al., "Time Behaviour of Heat Diffusivity during L-H-L Transitions in JT-60U", JAERI-Research 95-060 (1995).

[3.6] H. Shirai, T. Takizuka, M. Azumi, Proc. of International School of Plasma Physics, Varenna, Italy, 1993, (SIF, Bologna, 1993) p.33.

Table 3.1 Plasma parameters and $\delta\chi$ values

shot No	t (s)	I_p (MA)	B_t (T)	r	$\delta\chi_e$ (m^2/s)	$\delta\chi_i$ (m^2/s)
E16130	7.17	3.0	4.2	0.64	+ 0.60	
E17058	8.38	3.5	4.2	0.56		+0.55
				0.61	+0.65	
				0.71	+0.85	
E17060	8.49	3.5	4.2	0.63		+0.58
				0.73	+0.77	
E17038	7.15	2.0	4.2	0.55		-0.64
				0.63		-0.93
				0.63	-0.65	
E17298	5.71	1.5	2.5	0.44		-0.85
				0.52		-1.3
				0.60		-2.0
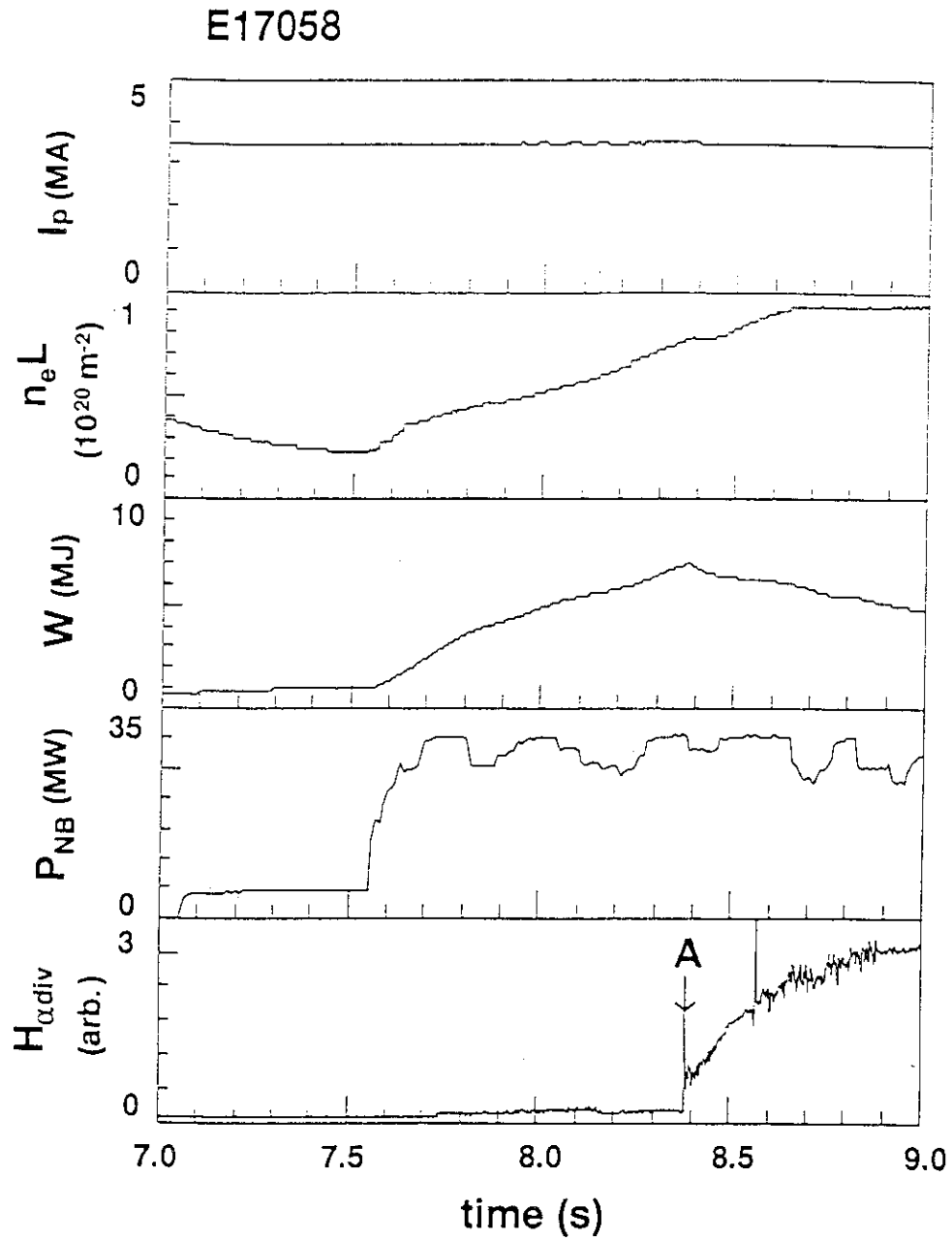
E17058

Fig. 3.1 Waveforms of a hot ion H-mode pulse E17058 (3.5 MA / 4.2 T). The growth of W is interrupted by a clear H-L transition at the time A.
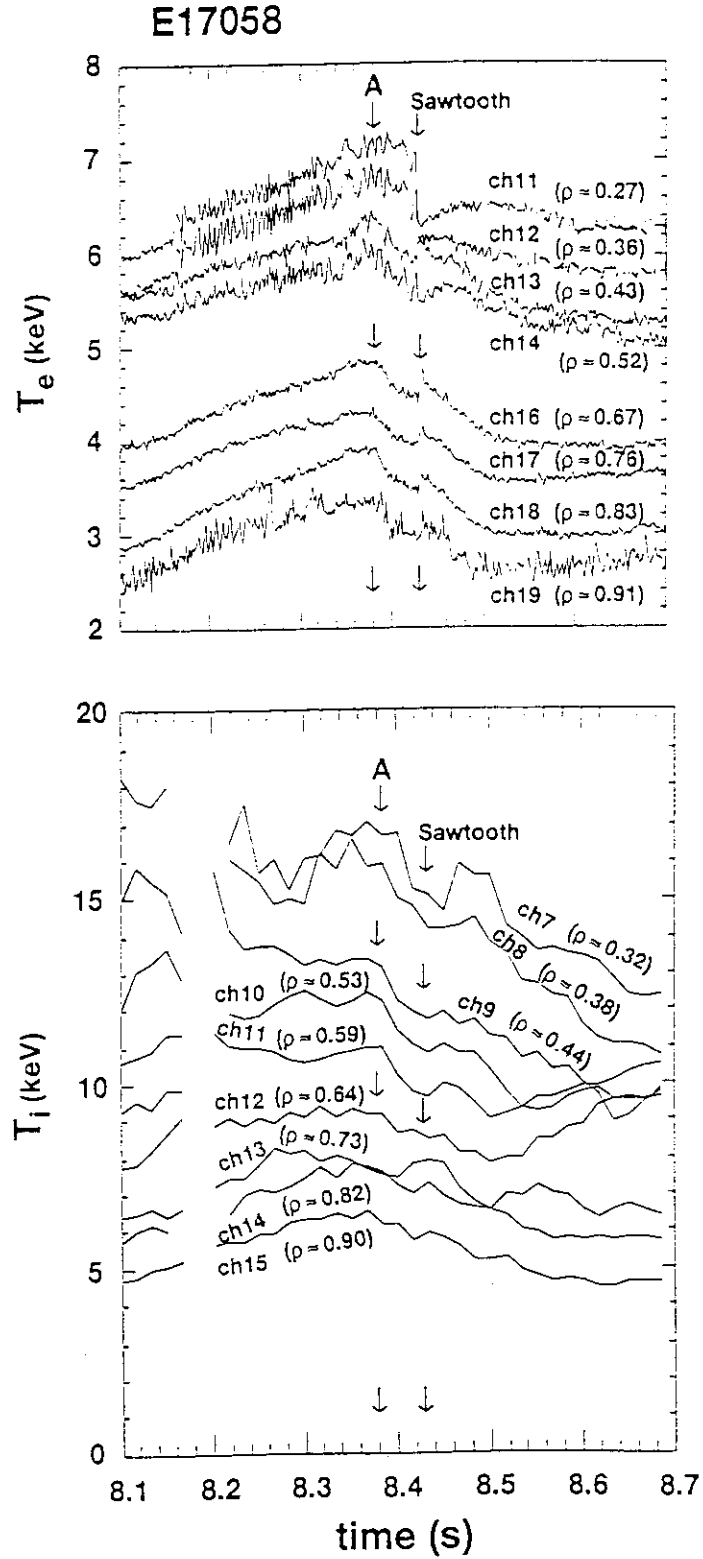
E17058

Fig. 3.2 Time evolutions of $T_e(\rho, t)$ and $T_i(\rho, t)$ for E17058 pulse. In the region $0.43 < \rho <$ 0.83, T_e varies simultaneously after A, while in the central region $\rho < 0.36$, T_e is changed slowly. T_i behaves similarly to T_e.
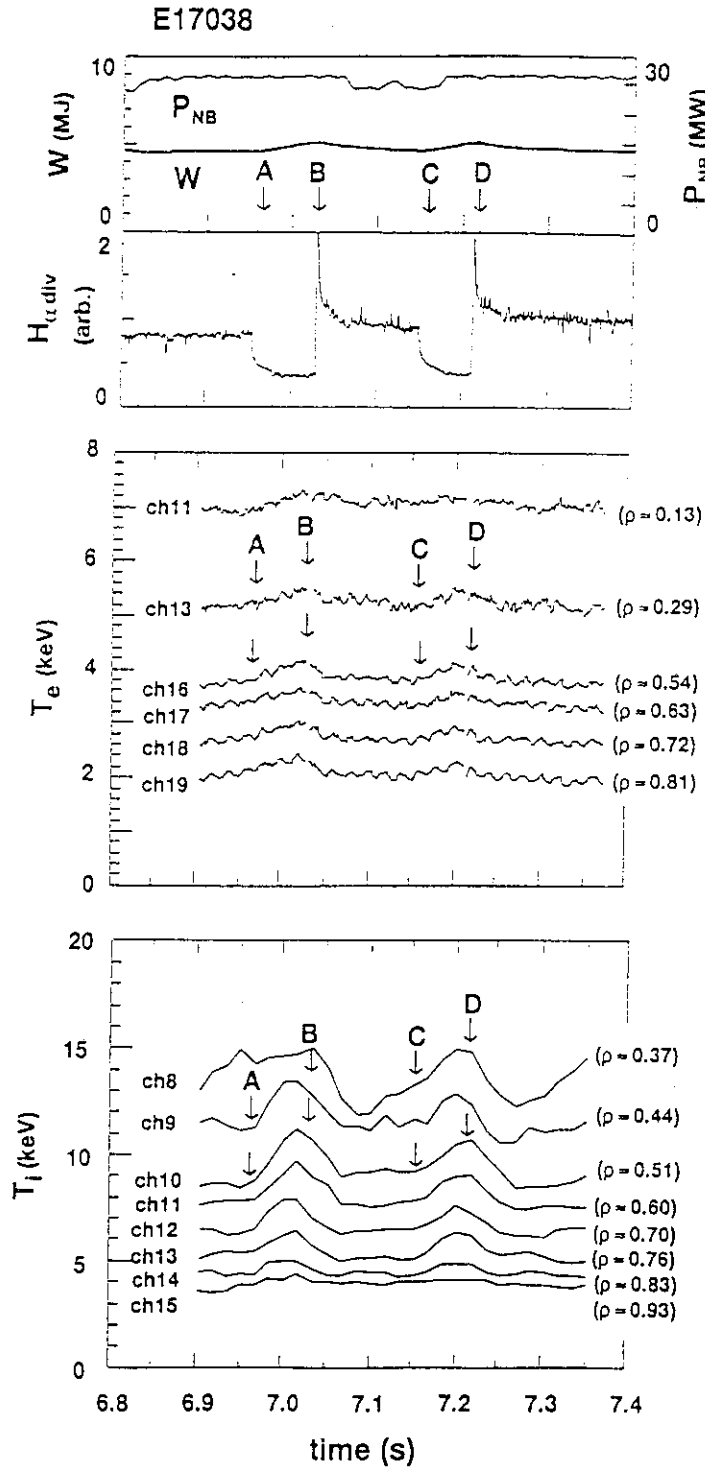
Fig. 3.3 Evolutions of W, P_{NB}, $H\alpha_{div}$, $T_e(\rho, t)$, and $T_i(\rho, t)$ for a hot ion H-mode pulse
E17038 with low I_p (2 MA / 4.2 T). Clear L-H and H-L transitions are observed and
two short H-mode phases appear. Simultaneous response of T_e with W and $H\alpha_{div}$ is
clearly seen over $0.3 < \rho < 0.8$. Simultaneous response of T_i is also seen.

4. Time Evolution of Transport Properties in JT-60U H-mode Plasmas with Improved Core Confinement

Hiroshi SHIRAI, Tomonori TAKIZUKA, Yoshihiko KOIDE, Yutaka KAMADA,

Shinichi ISHIDA, Masahiro MORI, Osamu NAITO, Masayasu SATO, Nobuaki ISEI,

Takeshi FUKUDA, Yasunori KAWANO, Toshio HIRAYAMA, Masafumi AZUMI

4.1 Introduction

One of the major objectives of H-mode experiments in JT-60U is to obtain high confinement plasmas. They were obtained by a high NBI power ($P_{inj} \geq 20$ MW) and high toroidal field ($B_t = 4.0$ T). These high confinement plasmas have a feature of the improved core confinement (ICC) with $T_i(0) \geq 20$ keV, $T_i(0)/T_e(0) \geq 2$ and high H factor (≥ 2). Hereafter we call them "ICC plasmas". The "high T_i H-mode plasmas" [4.1] and "high β_p H-mode plasmas" [4.2] are categorized in ICC plasmas. The ion thermal diffusivity, χ_i, substantially decreases in the plasma core region to the neoclassical level [4.3]. In some ICC plasmas an internal transport barrier (ITB) was formed [4.4]. Accross the ITB, the ion temperature increases by several keV.

Usually the first L-H transition of ICC plasmas occurs when plasma profiles are not yet in the steady state. Since the improvement of core confinement and the L-H transition occur simultaneously, the local transport analysis including the time evolution of density and temperature is necessary to identify the H-mode effect on the transport in ICC plasmas.

Several hundreds milliseconds after the first L-H transition, ELM activity starts in most of the ICC H-mode plasmas and the stored energy is saturated or gradually decreased. In some ICC H-mode plasmas, on the other hand, short period (~ 100 ms) of ELM-free H-mode phase and L-mode phase appear alternately after the saturation of the stored energy. We call this phenomenon "repetitive L-H-L transitions" in this paper. The stored energy and the local T_e and T_i values change simultaneously at L-H and H-L transitions [4.5]. The change rate of these variables is much larger than that at the first L-H transition. The repetitive L-H-L transitions were observed after the confinement improvement is well developed.

In this paper, the thermal confinement and local transport properties in relation to the first L-H transition and the repetitive L-H-L transitions appeared in ICC H-mode plasmas are analyzed.

4.2 Numerical calculation method

Profiles of electron and ion thermal diffusivities, χ_e and χ_i, are evaluated from the profile data of n_e, T_e, T_i, P_{rad}, P_{abs} and so forth. We use 1.5 dimensional time transient

tokamak transport analysis code, TOPICS, with 1D Fokker-Planck (FP) code which includes the effect of delayed heating by fast ions. In JT-60U plasmas, however, the ripple loss of beam ions cannot be neglected. An Orbit Following Monte Carlo (OFMC) code is used to evaluate the power deposition profile. Thus the deposition profile of NBI is calculated by OFMC and the total power is adjusted to the results of FP.

At the L-H and H-L transitions, we evaluate the improvement and degradation of the thermal confinement together with the local transport analysis. The scaling of the thermal stored energy, W_{th}, in JT-60 ohmically heated plasmas and NBI heated L-mode plasmas is given as follows [4.3],

$$W_{th}^{scaling}(MJ) = 0.026 \; M_i^{0.3} \; \kappa^{0.87} \; R^{1.44}(m) \; a^{0.93}(m) \; B_t^{0.39}(T) \; I_p^{0.5}(MA)$$
$$n_e^{0.5}(10^{19}m^{-3}) \; P_{net}^{0.33}(MW) \; .$$

When W_{th} varies in time, we put $P_{net} = P_{abs} - dW_{th}/dt$. Here we define the "TH factor" (Thermal H factor) by $W_{th}^{exp}/W_{th}^{scaling}$. The ratio of the beam stored energy, W_{beam}, to the total stored energy is considerably large (≥ 0.3), especially at the beginning of the NBI heating in ICC plasmas. Therefore we do not use the "H factor" based on ITER89 power scaling because it is not appropriate for evaluating the transport and thermal confinement properties.

4.3 Transport properties before and after the first L-H transition

In this subsection, we study the dynamic changes in local transport and global confinement properties before and after the first L-H transition of an ICC plasma when the confinement continues to improve.

Figure 4.1 shows the waveform of shot E16168 ($I_p = 3.5$ MA, $B_t = 4.2$ T, $q_{eff} = 3.2$, $R = 3.2$ m, $a = 0.84$ m, $\kappa = 1.65$, $V = 69$ m^3). The line integrated electron density, n_eL (L is about 2.4 m), the injected NBI power, P_{inj}, the net power, P_{net}, the stored energy measured by diamagnetic loop, W_{dia}, the D_α from the divertor region, $D_{\alpha div}$, and the TH factor are shown. A L-H transition (first transition) is clearly seen at t = 8.5 s. The ELM activity starts from t = 9.08 s and W_{dia} begins to decrease gradually. In the ohmic heating phase, TH factor is almost unity. At the L-H transition TH factor jumps from 1.31 to 1.51. After the L-H transition, TH factor keeps increasing up to 1.73 on a time scale of the thermal energy confinement time, τ_E^{th}. After the ELM starts, TH factor decreases dramatically to the level before the L-H transition.

The time evolution of n_e, T_e and T_i profiles of shot E16168 is shown in Fig. 4.2 . The ITB is seen around r/a = 0.4 ~ 0.5 in the T_i profile. At t = 8.4 s, the ITB once disappears because of the beam fault. After that the ITB is formed again, and the central T_i reaches

about 25 keV. At the L-H transition, T_i increases over the whole plasma. During the NBI heating phase, n_e and T_e keep increasing. However, their profiles change little after the L-H transition.

Figure 4.3 shows the comparison of χ_e and χ_i profiles at (a) before the transition (t = 8.45 s), (b) after the transition (t = 8.55 s), (c) just before ELM (t = 9.0 s) and (d) during ELM (t = 9.1 s). At the L-H transition, χ_i decreases over the whole plasma. The time scale of the χ_i decrease is much smaller than τ_E^{th} (τ_E^{th} at (a) is about 300 ms). As for χ_e, it decreases in the outer region (r/a $\geq$ 0.8), while it does not change too much in r/a $\leq$ 0.8 .

During H-mode phase, χ_i increases gradually. At the time (c), both χ_e and χ_i are almost the same as those at (a) and τ_E^{th} becomes about 330 ms. Since P_{net} at (c) is about twice as large as that at (a) and both T_e and T_i increase during H-mode phase, the improvement of the confinement proceeds during the H-mode phase in the sense that there is no power degradation.

Thus the evolution of local transport and the confinement improvement has two different time scales at the first L-H transition and the successive H-mode phase: fast change (much smaller time scale of τ_E^{th}) at the L-H transition and the succeeding slow change (time scale of τ_E^{th}).

After the ELM activity starts, χ_i increases over the whole plasma and TH factor drops very fast to the level before the L-H transition. At the same time χ_e slightly increases. These are shown in lines (d) in Fig. 4.3.

4.4 Transport properties during the repetitive L-H-L transitions

In this subsection, we study the case of repetitive L-H-L transitions after the confinement improvement is well developed.

Figure 4.4 shows the waveform of shot E16107 during the repetitive L-H-L transitions phase. Plasma parameters in the shot E16107 are I_p = 2.7 MA, B_t = 4.2 T, q_{eff} =4.5, R = 3.2 m, a = 0.91 m, κ = 1.5, V =72 m^3, n_e = 2.3 x 10^{19} m^{-3}, $T_e(0)$ $\approx$ 7 keV and $T_i(0)$ $\approx$ 22 keV. The NBI heating begins at t = 8.0 s and the first L-H transition occurs at t = 8.5 s. The time evolution of $D_{\alpha div}$ shows that L-mode phase and H-mode phase appear alternately. Both W_{dia} and n_eL begin to increase at the L-H transition and decrease at the H-L transition. The local T_e and T_i values over the whole plasma (0.2 $\leq$ r/a $\leq$ 0.9) also begin to change at the transitions within the time resolution of measurement. The TH factor changes from 1.2 to 1.47 at (e) in Fig. 4.4 and from 1.74 to 1.26 at (f). The time scale of these change is much smaller than τ_E^{th}. During H phase, TH factor increase as the same as shown in the former subsection.

Figure 4.5 shows the profiles of n_e, T_e and T_i in the H-mode phase and L-mode phase of shot E16107. The corresponding χ_e and χ_i profiles (thick line to the H phase and thin line

to the L phase) are calculated as shown in Fig. 4.6. Both χ_e and χ_i changes over the whole plasma.

4.5 Conclusion

We have studied the time evolution of global confinement and local transport properties in ICC H-mode plasmas with $T_i(0) \geq 20$ keV in JT-60U. At the first L-H transition when both T_e and T_i keep increasing and the confinement continues to improve, TH factor and χ_i changes in two different time scale: much smaller time scale of τ_E^{th} at the L-H transition and the succeeding slow change on a time scale of τ_E^{th}. At the repetitive L-H-L transitions, when the confinement improvement is well developed, TH factor and χ changes on a much smaller time scale than τ_E^{th}.

We continue the transport study of ICC H-mode plasmas to clarify the mechanism of fast and slow changes in the global confinement and local transport properties. Difference of χ_e behaviour in shot E16168 (small change between L- and H-phases) and in shot E16107 (remarkable change) is not resolved. The evolution of χ in the edge barrier was not studied here because of lack of edge profile data. These are future problems to be clarified.

References

[4.1] M. Kikuchi, H. Shirai, T. Takizuka, Y. Kamada *et al., Proc. 14th Conf. on Plasma Physics and Controlled Nucl. Fusion Research, Würzburg, 1992*, Vol. 1, p. 189.

[4.2] S. Ishida, M. Matsuoka, M. Kikuchi, S. Tsuji *et al.*, ibid. Vol. 1, p. 219.

[4.3] H. Shirai, T. Takizuka, M. Kikuchi, M. Mori *et al., Proc. 15th Conf. on Plasma Physics and Controlled Nucl. Fusion Research, Seville, 1994*, IAEA-CN-60/A-2-III-6.

[4.4] Y. Koide, M. Kikuchi, M. Mori, S. Tsuji *et al.*, Phys. Rev. Lett. **72** (1994) 3662.

[4.5] S.V. Neudatchin, H. Shirai, T. Takizuka, N. Isei *et al.*, The Time Behaviour of the Heat Diffusivity during L-H-L Transitions in JT-60U, *Proc. 22nd Eur. Conf. on Controlled Fusion and Plasma Physics, Bournemouth, 1995*.
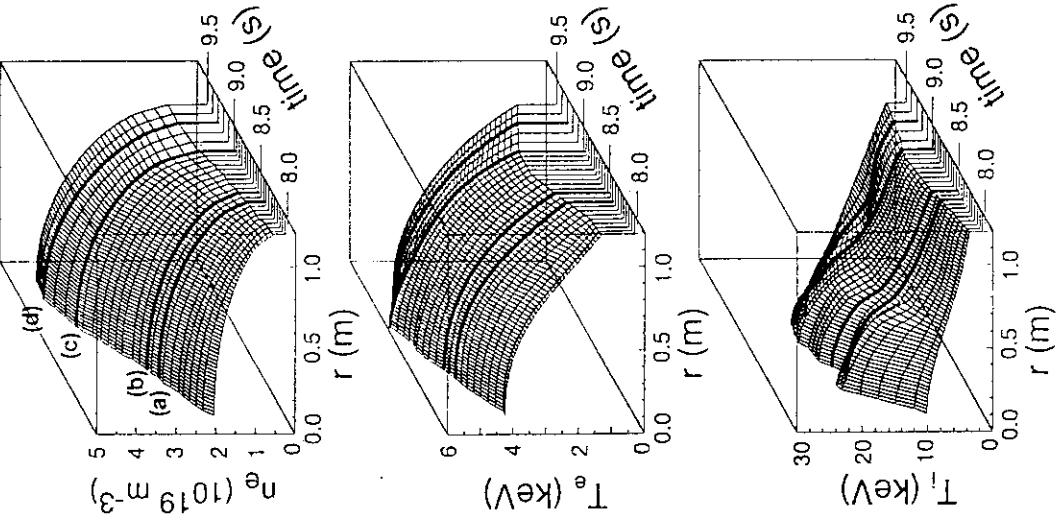
Fig. 4.2 Time evolution of n_e, T_e and T_i profiles in shot E16168.
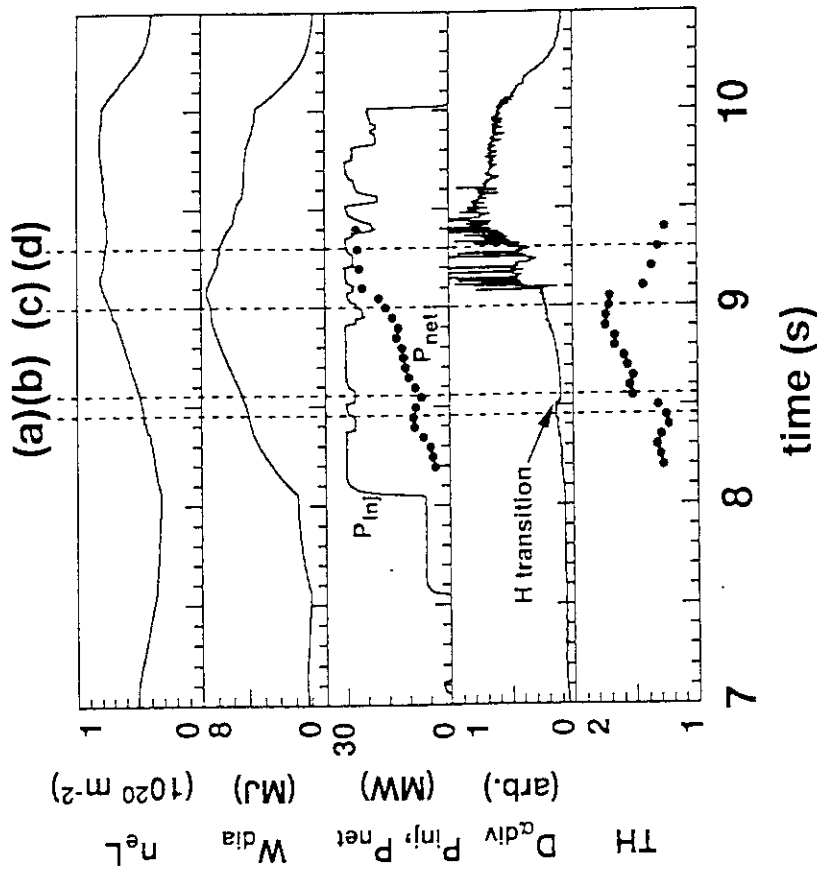
Fig. 4.1 Waveforms of shot E16168 with $I_p = 3.5$ MA, $B_t = 4.2$ T.

Fig. 4.4 Waveforms of shot E16107 with $I_p = 2.7$ MA, $B_t = 4.2$ T.

Fig. 4.3 Profiles of χ_e and χ_i for various time points in shot E16168.

Fig. 4.6 Profiles of χ_e and χ_i in the H-mode phase and L-mode phase of shot E16107.

Fig. 4.5 Profiles of n_e, T_e and T_i in the H-mode phase and L-mode phase of shot E16107.

5. Non-dimensional Transport Experiment in JT-60U

Tomonori TAKIZUKA, Hiroshi SHIRAI, Yutaka KAMADA, Takeshi FUKUDA,
Katsuhiko TSUCHIYA, Shinichi ISHIDA, Masahiro MORI

5.1 Introduction

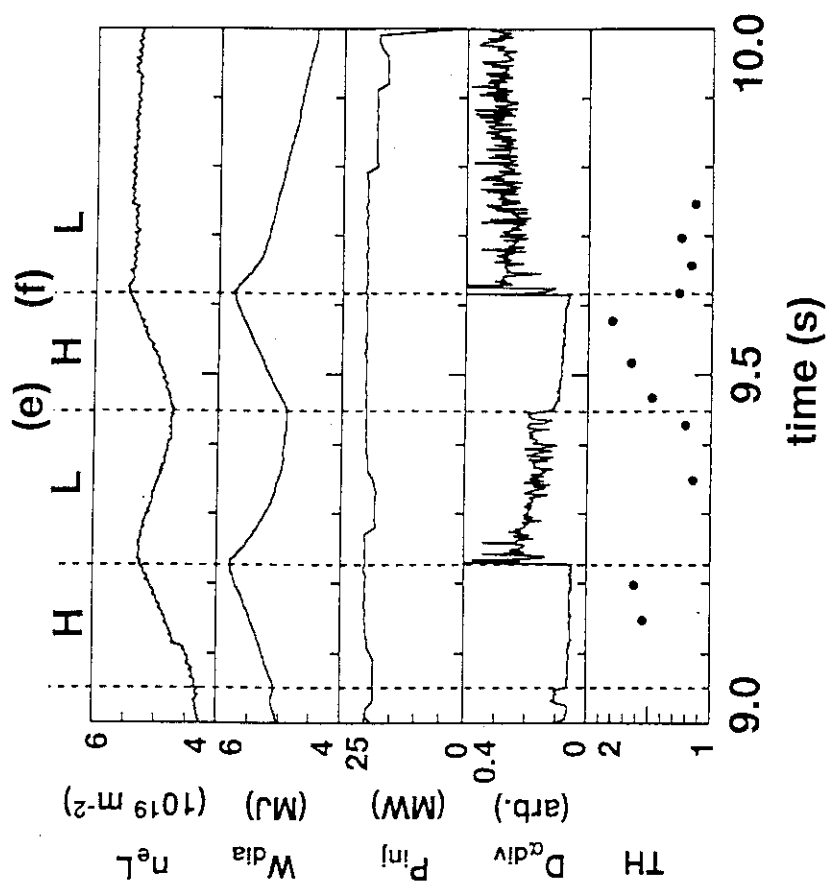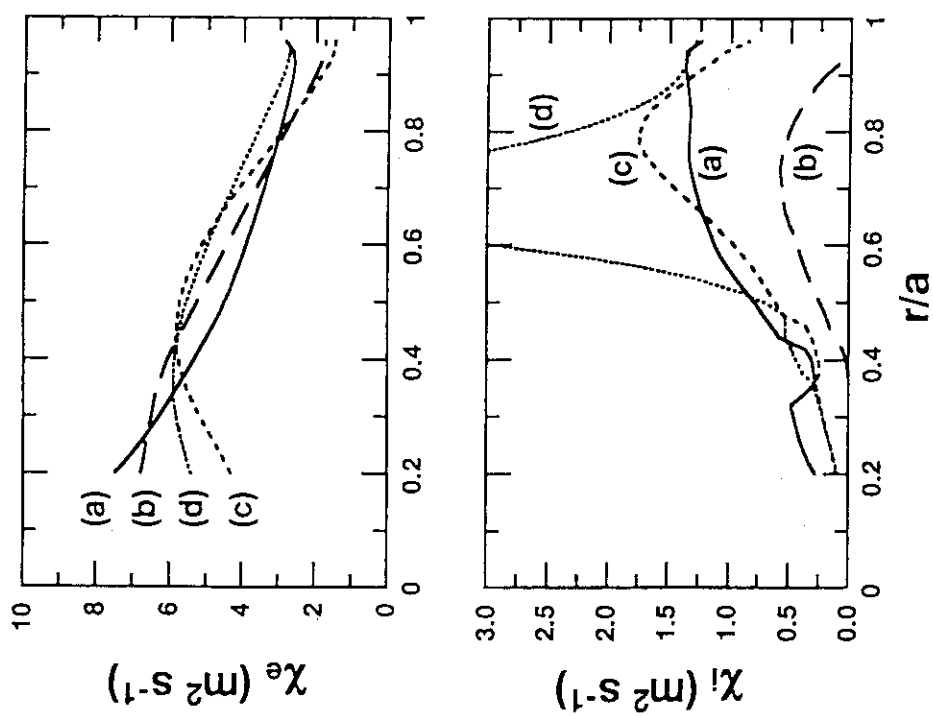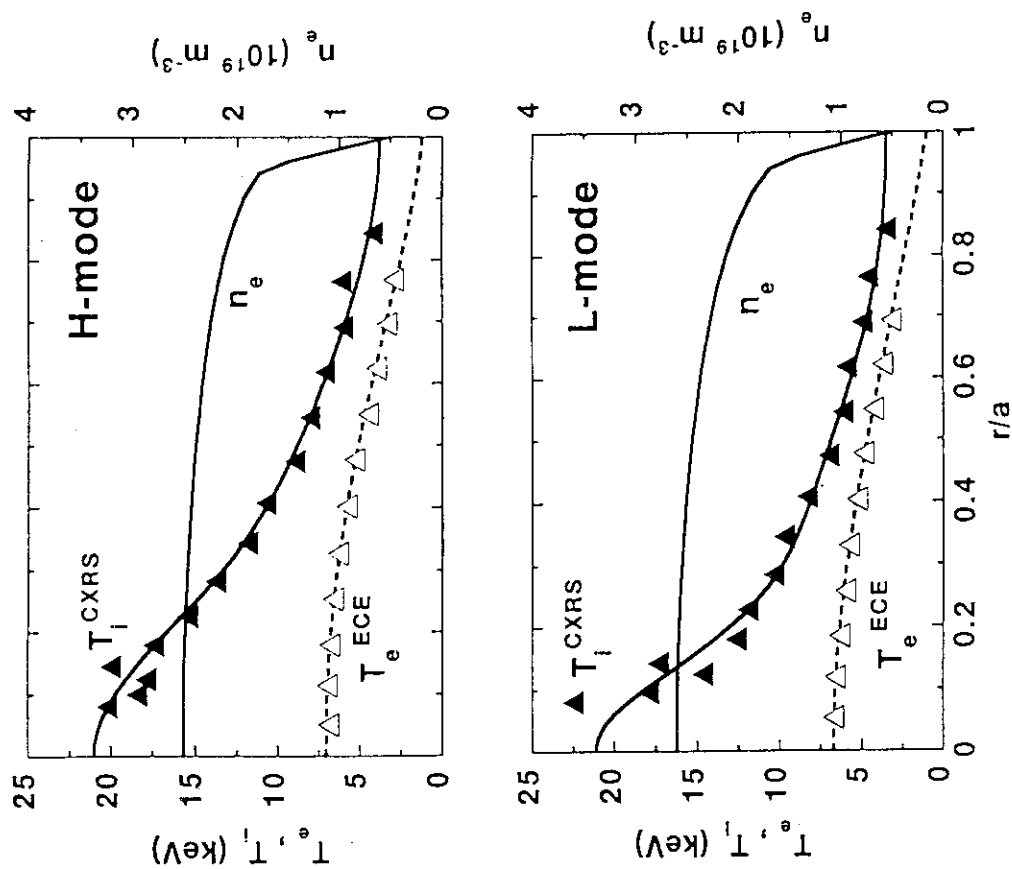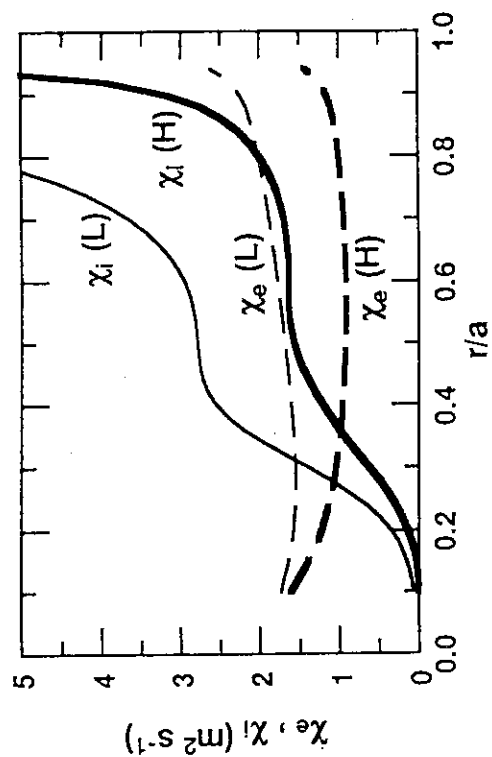In the thermonuclear fusion research and development, ITER EDA project is one of the most important projects, which aims to demonstrate an engineering design of a thermonuclear experimental reactor. It is required for the performance of ITER that ITER should have a confinement capability to reach controlled ignition and extended burn for a duration longer than characteristic time scales of plasma processes and plasma wall interactions [5.1]. The ELMy H-mode confinement is appropriate for satisfying this requirement, and is considered to be sustained in ITER. The expected performance of the confinement is based on the scaling law. At the present time, a following scaling law has been recommended by ITER Physics R&D Expert Group for ELMy H-mode confinement in ITER [5.2];

$$\tau_{th}^{ELMy} = 0.85 \, \tau_{th}^{ELM\text{-}free} \, , \tag{5.1}$$

where the thermal energy confinement time for ELM-free H-mode, $\tau_{th}^{ELM\text{-}free}$, was given by the ITER H-mode Database Working Group [5.3] as

$$\tau_{th}^{ELM\text{-}free} = 0.036 \, M^{0.41} \, I_p^{1.06} \, B_t^{0.32} \, n_e^{0.17} \, R^{1.9} \, a^{-0.11} \, \kappa^{0.66} / P_{net}^{0.67} \, . \tag{5.2}$$

The units in the scaling expression are following; confinement time τ is in s, plasma current I_p in MA, toroidal field B_t in T, line averaged density n_e in 10^{19} m^{-3}, major radius R in m, minor radius a in m, and net power P_{net} is in MW. The ion mass number is denoted by M and the ellipticity by κ.

The thermal energy confinement time τ_{th} is considered to be related to the heat diffusivity χ in a plasma as $\tau_{th} \propto a^2 / \chi$. It is also related to the stored thermal energy $W_{th} \propto a^2 \, R \, n_e \, T$ as $\tau_{th} = W_{th} / P_{net}$, where T is the plasma temperature. Replacing P_{net} with T by using above relations and Eqs. (5.1) and (5.2), we obtain a expression of χ correspond to the H-mode confinement with and without ELM;

$$\chi^{H\text{-}mode} \propto (T / eB_t) \, \rho_*^{0.73} \, \beta^{1.205} \, \nu_*^{0.285} \, . \tag{5.3}$$

A small correction in Eq. (5.2) is necessary for the dimensional correctness, and the size scaling of $R^{1.79} \, (R/a)^{0.11}$ is replaced to that of $R^{1.775} \, (R/a)^{0.11}$. In the relation (5.3), (T / eB_t) is the Bohm diffusion coefficient and other quantities, ρ_*, β and ν_*, are the non-dimensional

variables. The normalized gyro radius ρ_* is proportional to $T^{0.5}/R\,B_t$, the beta value β to $n_e\,T/B_t^2$, and the collisionality ν_* to $R\,n_e/T^2$. Since the dependence of $\chi^{H\text{-mode}}$ on ρ_* is nearly linearly proportional, confinement property of H-mode is like a gyro-Bohm type.

As for the L-mode confinement, ITER89-P scaling of the total energy confinement time τ_E corresponds to a Bohm type confinement with $\chi \propto (T/eB_t)\,\rho_*^0\,\beta^{0.555}\,\nu_*^{0.275}$. The improvement in the confinement has been evaluated with the use of H-factor ($= \tau_E/\tau_E^{ITER89P}$ or $= \tau_{th}/\tau_E^{ITER89P}$). The values of b and ν_* in the ITER plasma with R^{ITER} and B_t^{ITER} will be almost the same as those attained in the present tokamak plasmas with R and B_t. For this situation, the value of ρ_* in ITER, ρ_*^{ITER}, will become smaller than the present ρ_* value;

$$(\rho_*^{ITER}/\rho_*) \approx (R/R^{ITER})^{5/6}\,(B_t/B_t^{ITER})^{2/3}\;. \tag{5.4}$$

Therefore, if the ELMy H-mode confinement is really a Gyro-Bohm type, H-factor in ITER will be larger than that obtained in the present experiments.

In order to confirm above physics base of ITER design, non-dimensional transport experiments for ELMy H-mode plasmas were required as ITER physics research needs [5.4]. The experiments, then, have been carried out in DIII-D [5.5] and in JET [5.6]. Non-dimensional plasma parameters except ρ_* have been chosen like ITER parameters. The gyro-Bohm type confinement was found in DIII-D, while the Bohm type confinement was found in JET. In this paper, we report the result of the non-dimensional transport experiments performed in JT-60U.

5.2 Experimental Results

We compare three ELMy H-mode shots with different B_t and I_p values; shot E23555 ($B_t = 1.5T$ / $I_p = 0.9MA$), shot 23556 (2.5T / 1.5MA) and shot E23559 (3T / 1.8MA). The neutral beam of deuterium is injected into deuterium plasmas. The plasma configurations of these discharges are nearly similar with each other as shown in Fig. 5.1; $R \approx 3.27$ m, $a \approx 0.82$ m, and $\kappa \approx 1.6$. The safety factor at the 95% flux surface q_{95} is chosen as an ITER condition ($q_{95} \approx 3$). Though one of the major aims of the experiments is to investigate the ρ_* scaling in the ITER relevant plasma condition, an important non-dimensional parameter of the aspect ratio of JT-60U, $R/a \approx 4$ is different from the ITER's, $R/a = 8.1m/2.8m \approx 2.9$. Therefore, values of total β and poloidal β_p in JT-60U cannot simultaneously be set the same as in ITER, and only β_p value is set the same as in ITER. The collisionality is evaluated as that of passing particles,

$$\nu_* = \nu\,q_{95}R/\nu_{th} \approx 2 \times 10^{-3}\,n_e\,q_{95}R/T^2\;, \tag{5.5}$$

and the normalized gyro radius as that of a poloidal gyro radius,

$$\rho_* = m_e v_{eth} / eB_p R \approx 10^{-4} T^{0.5} q_{95} / \kappa^{0.5} a B_t , \qquad (5.6)$$

where n_e is in 10^{19} m^{-3}, R in m, a in m, T in keV, and B_t is in T. The ratio of ion temperature T_i to electron temperature T_e is nearly unity as shown in Fig. 5.2 for B_t = 2.5T. The T_i (circles in the figure) is measured by charge-exchange recombination spectroscopy (CXR), and the Te (squares) is measured by ECE Fourier transform spectrometer (ECE). This equi-temperature condition is one of ITER relevant conditions. The triangularity $\delta \approx 0.1$ in JT-60U is rather small compared with that in ITER, $\delta \approx 0.4$.

Figure 5.3 shows the wave forms of three discharges. The line integrated electron density, $n_e L$ (L is about 2.2 m), the stored energy measured by diamagnetic loop, W_{dia}, the injected neutral beam power, P_{NBI}, and the H_α intensity from the divertor region, $H_{\alpha div}$, are demonstrated. In order to set values of β and ν_* similar to the ITER values, the density is controlled by gas puffing and the neutral beam power is changed stepwise in time. The times of comparison, at which β and ν_* are similar to ITER's, are indicated by broken lines. The L-H transitions for all cases occur enough before the times of comparison. In all cases, ELMy H-modes are obtained.

The results of experiment are summarized in Table 5.1, where ITER parameters are also listed for comparison. The absorption power P_{abs} is given by using a Orbit-following Monte-Carlo code to estimate the ripple loss. Values of T is those near r/a = 0.5. The thermal stored energy is calculated from profile data, n_e, T_i^{CXR} and T_e^{ECE}, and from the consistency check with W_{dia}, neutron emission rate and so on. Values of thermal poloidal-beta β_{pth} are almost similar, while ν_* for B_t = 1.5T is higher than others due to the difficulty in the control of low density. We consider that this difference affects little the conclusion because the effect of ν_* on the transport may be much weaker than that of β.

The values of H-factor ($H = \tau_E / \tau_E^{ITER89P}$) are compared among three cases. The H-factor changes little during the decrease of ρ_* from 2.4 (B_t = 1.5T) to 1.8 (B_t = 2.5T), and it is reduced at B_t = 3.0T. This fact suggests that the confinement property of ELMy H-mode in JT-60U is never a Gyro-Bohm type, but is like a Bohm type. The comparison of H_H-factor ($H_H = \tau_{th} / \tau_{th}^{ELMy}$) shows the same conclusion: If the confinement is a Gyro-Bohm type, H_H-factor is nearly constant during the change of ρ_* value. In fact, however, H_H-factor is degraded by the decrease of ρ_*. Finally we compare the confinement time τ_{th} normalized by the Bohm confinement time $\tau_B \propto eB / T$. Values of this Bohm-normalized confinement time vary little during the change of ρ_* value. This result also suggests a Bohm type confinement of ELMy H-mode in JT-60U plasmas under the ITER relevant condition.

5.3 Discussion

The non-dimensional transport experiments shows that the confinement property of ELMy H-mode in JT-60U plasmas is a Bohm type under the ITER relevant condition. The values of H-factor in these plasmas are rather low compared with DIII-D and JET results. We discuss in this subsection why the H-factor is not high and why the confinement becomes a Bohm type.

5.3.1 Low H-factor in plasmas with $T_i/T_e \approx 1$

The values of H-factor are 1.42 for $Bt = 1.5T$, 1.39 for $Bt = 2.5T$, and 1.25 for $Bt = 3.0T$, which are rather low compared with those in DIII-D ($H = 1.5 - 2.0$) [5.5] and in JET ($H \approx 1.7$) [5.6]. The values of H_H-factor from 0.62 to 0.51 are also low.

In order to obtain the high H-factor in JT-60U plasmas, the high T_i condition ($T_i / T_e > 1$) has been inevitable. A scaling expression for the H-factor of high T_i H-mode in JT-60U was given as $H - 1 \propto (T_{i0}/T_{e0} - 1) n_e^{1.5}$ [5.7], where subscript 0 denotes the center value. The ratio T_{i0}/T_{e0} in the ITER relevant plasmas for the present experiments, however, is almost unity as already shown in Fig. 5.2. Therefore, high values of H-factor in the present plasmas are hardly attained.

5.3.2 Effect of ELM activity on the improvement

Non-dimensional transport experiment for ELMy H-mode in JT-60U has shown that the H-factor does not increase and the H_H-factor decreases with the increase of B_t. This result suggests that the ELMy H-mode confinement looks a Bohm type. The transport property of L-mode plasmas in JT-60U was found to be a Weak Gyro-Bohm type [5.8]. It is difficult to imagine that the spatial dependence of the heat diffusivity becomes a Bohm type one in H-mode plasmas. A Bohm type property may be observed when we compare plasmas with different parameters. The cause of this Bohm type property can be explained as the effect of ELMs, which become more active in a higher B_t plasma than in a lower B_t plasma.

An index of the ELM activity, β/ρ_*, was found in Ref. [5.9]. Giant ELMs start when this index exceeds a limit as was shown in Fig. 1(b) in Ref. [5.9]. As the input power increases and the value of β/ρ_* increases beyond the limit, the ELM frequency f_{ELM} becomes high. This tendency was clearly shown in Fig. 2(b) in Ref. [5.9] also. Throughout the non-dimensional transport experiments, the index is increasing with the increase of B_t (decrease of ρ_*), and f_{ELM} is also increasing. One can clearly see in Fig. 5.3 that f_{ELM} becomes higher in higher B_t plasmas. When f_{ELM} becomes higher, the improvement in the confinement can be degraded [5.9]. The relation between f_{ELM} and H-factor is shown in Fig. 5.4, which is the same as Fig. 9(a) in Ref. [5.9]. We suppose, therefore, that the feature of a Bohm type

confinement is caused by the suppression of improvement due to enhanced ELM activity during the increase of B_t .

5.4 Summary

We have carried out the non-dimensional transport experiments of ELMy H-mode in JT-60U under the ITER relevant condition. The results shows that the confinement property of the ELMy H-mode is a Bohm type. When B_t increases with constant β and decreasing ρ_*, an index of ELM activity, β/ρ_*, increases and ELMs become active. We suppose that this enhanced ELM activity suppresses the improvement in the H-mode confinement of a plasma with smaller ρ_*. This suppression can be the cause of the Bohm type confinement of ELMy H-mode in JT-60U.

In order to reduce the ELM activity, the increase of the triangularity δ of a plasma cross section can be efficient. We will perform the non-dimensional transport experiments in the high δ configuration of JT-60U.

Acknowledgment

References

[5.1]   ITER JCT, "ITER General Design Requirement Document" (1995).

[5.2]   ITER JCT, "ITER Interim Design Report" (1995).

[5.3]   ITER H Mode Database Working Group, Nucl. Fusion 34 (1994) 131.

[5.4]   ITER Physics Committee, ITER Physics Committee Meeting, Naka, 1994 .

[5.5]   C.C. Petty, T.C. Luce, K.H. Burrell et al., Phys. Plasmas 2 (1995) 2342.

[5.6]   J.G. Cordey, B. Balet, D, Campbell, et al., "ITER Simulation Experiment on JET of the H-mode Power Threshold, Confinement Scaling and β Saturation", 5th H-mode Workshop, Princeton, (1995).

[5.7]   T. Takizuka, M. Kikuchi, H. Shirai, "Scaling of High Ti H-mode Confinement in JT-60U", section 2 in this report.

[5.8]   H. Shirai, T. Takizuka, O. Naito et al., "Nondimensional Transport Study of JT-60U Plasmas", to be published in J. Phys. Soc. Japan.

[5.9]   Y. Kamada, K. Ushigusa, O. Naito et al., Plasma Phys. Contr. Fusion 36 Suppl. (1994) A123.

Table 5.1 Experimental results and comparison with ITER

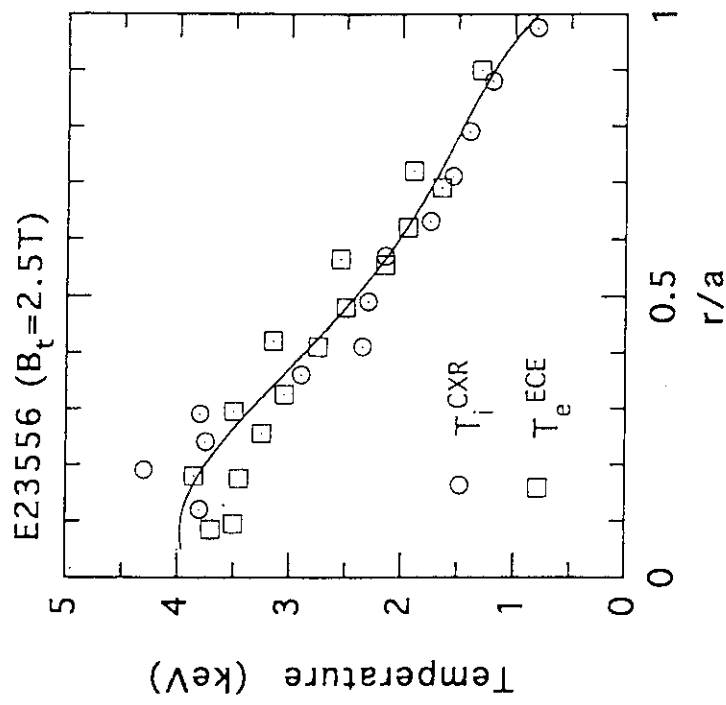|	JT60-U			ITER
R (m)	3.3			8.1
a (m)	0.82			2.8
V (m^3)	63			2000
Shot No.	E23555	E23556	E23559	
B_t (T)	1.5	2.5	3.0	5.7
I_p (MA)	0.9	1.5	1.8	21
q_{95}	3.0	3.0	3.0	3.0
P_{abs} (MW)	3.0	7.0	9.5	
n_e ($10^{19}m^{-3}$)	1.7	2.5	3.3	13
T (keV)	1.5	2.5	2.7	10
W_{th} (MJ)	0.52	1.32	1.83	
β_{pth}	0.43	0.40	0.39	0.5
ν_* (10^{-3})	13	8	8	4
ρ_* (10^{-3})	2.4	1.8	1.6	0.5
τ_{th} (s)	0.17	0.19	0.19	
H(ITER89P)	1.42	1.39	1.25	
H_H(ELMy H)	0.62	0.55	0.51	
(τ_{th} T/eB_t)$_{nor}$	0.95	1	0.89	

Fig. 5.2 Temperature profile for B_t = 2.5 T. Circles denote T_i measured by CXR and squares denote T_e measured by ECE. They have nearly the same values.
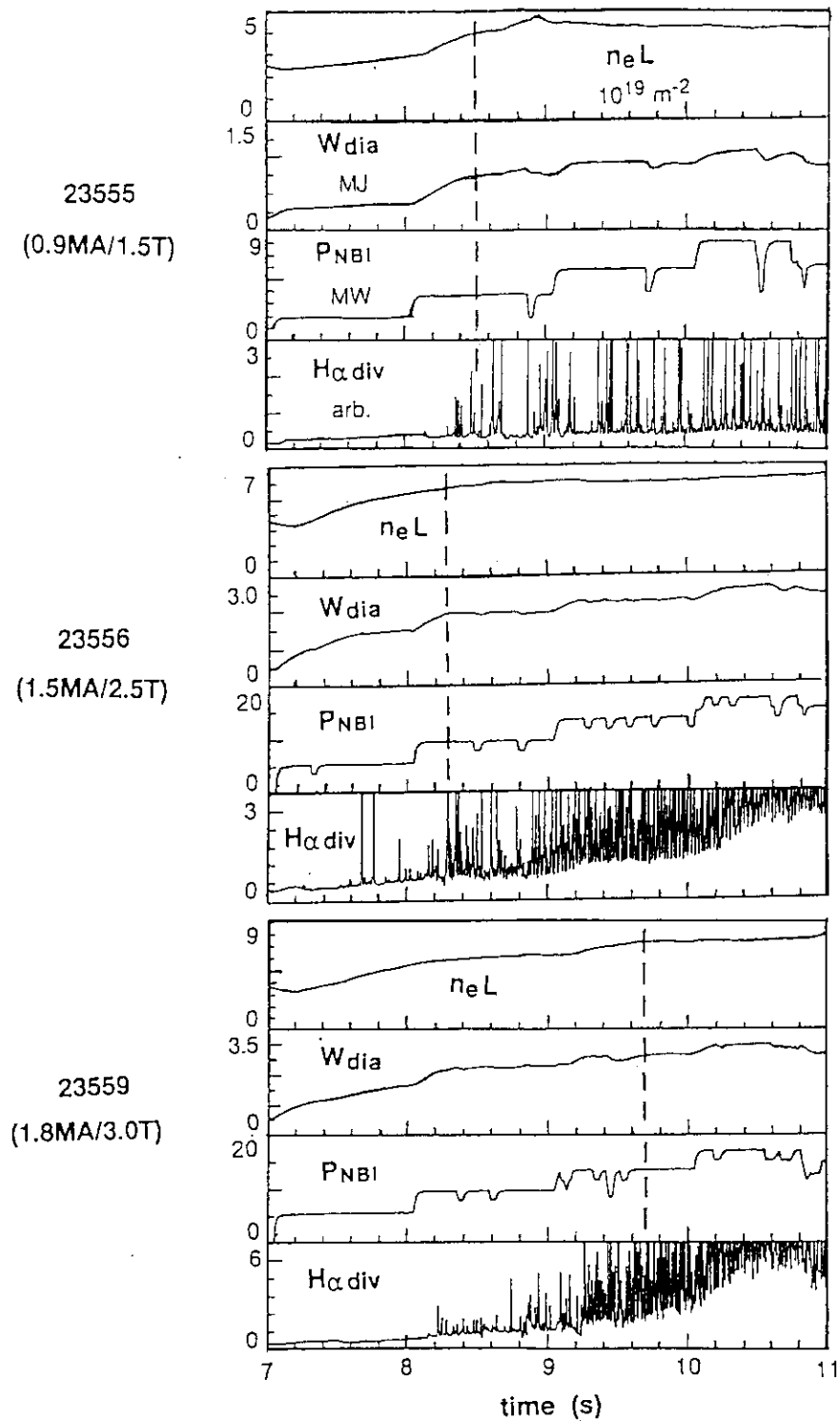

Fig. 5.1 Plasma configuration in JT-60U.

Fig. 5.3 Time evolution of n_eL, W_{dia}, P_{NBI}, and $H_\alpha div$ for three shots with B_t = 1.5T, 2.5T, and 3.0T. Dashed lines denote the times of comparison. ELMs become active in a higher B_t plasma.
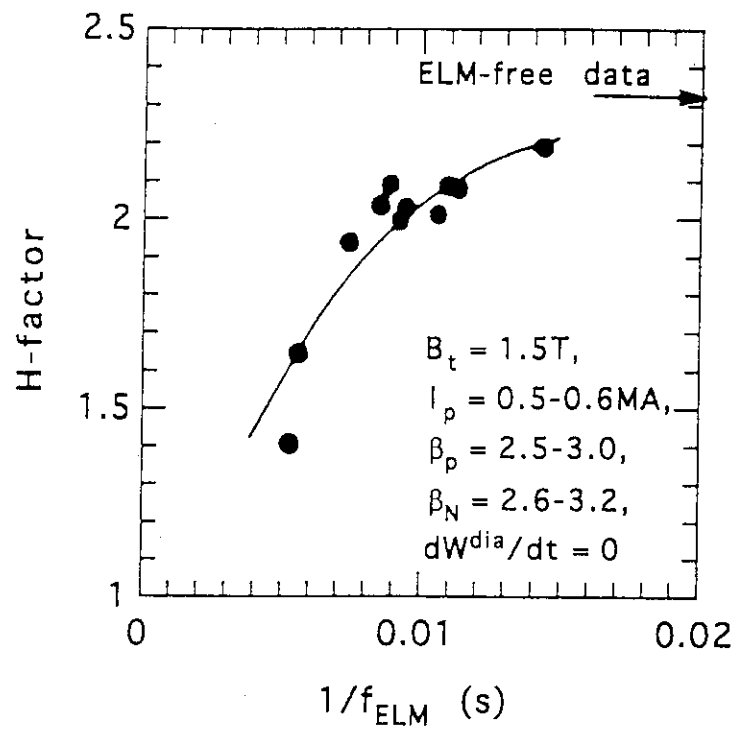
Fig. 5.4 Relationship between f_{ELM} and H-factor.

6. Threshold Power for H-mode Transition in JT-60U Plasmas

Masayasu SATO, Takeshi FUKUDA, Tomonori TAKIZUKA, Yutaka KAMADA,

Katsuhiko TSUCHIYA, Hiroshi SHIRAI, Shinichi ISHIDA, Masahiro MORI

6.1 Introduction

Fusion reactors, such as ITER, are designed based on the H-mode confinement scheme. Threshold power (P_{th}) for the H-mode transition is one of the key issues for design of reactors. Following scaling of P_{th} was proposed so far [6.1]; $P_{th}^{ITER} \propto \bar{n}_e$ B_t S, where $\bar{n}_e$, B_t and S are line-averaged electron density, toroidal magnetic field and the plasma surface area, respectively. Although scaling of confinement time depends on the plasma current (I_P) [6.2], the dependence of P_{th} on I_P have been considered to be very weak. Here, dependence of P_{th} on I_P and effective safety factor (q_{eff}) have been carefully studied, as well as its dependence on B_t and $\bar{n}_e$ in single-null divertor operation with $R \sim 3.3$ m and $a \sim 0.83$ m [6.3].

6.2 Threshold power

In neutral beam heated JT-60U plasma with boronized vessel walls, parametric scans were performed in order to reappraise the dependence of P_{th} on I_P (0.9MA $\leq I_P \leq$ 2.4MA), q_{eff} (3.6 $< q_{eff} <$ 10.2), B_t (1.5T $\leq B_t \leq$ 4.1T) and $\bar{n}_e$ (0.7 x 10^{19}m^{-3} $\leq \bar{n}_e \leq$ 2.8 x 10^{19}m^{-3}). Performed parametric scans are categorized into four cases; (1) I_P scan with B_t = const and $\bar{n}_e$ ~ const, (2) B_t scan for I_P = const and $\bar{n}_e$ ~ const, (3) I_P and B_t scan for q_{eff} = const and $\bar{n}_e$ ~ const, and (4) $\bar{n}_e$ scan for I_P = const and B_t = const. The discharge regions are shown in Fig. 6.1. The plasma parameters are as follows: $2 \leq Z_{eff} \leq 5.5$, 0.2MW $\leq P_{rad} \leq$ 2.2MW where P_{rad} is radiated power from main plasma.

Since recycling condition of the wall and neutral particle behaviors are found to influence the transition criteria [6.4], the experiments were carried out in continuous discharges (~70 discharges) with a fixed small ripple-loss configuration which is shown in Fig. 6.2. The ripple loss is less than 20%. Data of P_{th} from only discharges with low recycling have been analyzed in this paper. The typical time evolution of the plasma parameters is shown in Fig. 6.3. In order to evaluate the P_{th} for accuracy, neutral beams were injected into plasma in time dependent shape of step. Net power (P_{net}) is evaluated based on following equation; P_{net} = (1-Freion)(Pinj-Pshine) +POH - dW/dt, where Pinj, Pshine, POH, Freion and W are power of injected NBI, shinethrough, ohmic, fraction of reionization and diamagnetic stored energy.

The dependence of observed P_{th} on density is shown in Fig. 6.4 for the region of $\bar{n}_{e19}$ (10^{19}m^{-3}) ≥ 1.2. The region of density was restrained, because there was a threshold density below which the H-mode is never obtained for minimum P_{th} [6.5]. Obtained scaling is $P_{th} \propto \bar{n}_e^{0.5}$ for the region. The density dependence of P_{th} was weaker than P_{th}^{ITER}.

Concerning the magnetic field strength, dependence of $P_{th} / \overline{n_e}^{0.5}$ on the toroidal magnetic field is shown in Fig. 6.5. It was found that P_{th} depends on the toroidal magnetic field and its power factor was about 1 in a wide range of B_t from 1.5 to 4.1T.

The density dependence of $P_{th} / (\overline{n_e}^{0.5} B_t)$ is shown in Fig. 6.6. The function of $f(\overline{n_e})$ was assumed to be around unity for $\overline{n_e}_{19} \geq 1.2$ and $f = 1.2/\overline{n_e}_{19}$ for $\overline{n_e}_{19} \leq 1.2$. The threshold power increases with the decreasing density in the range of $\overline{n_e}_{19} \leq 1.2$. It was confirmed again that there is a threshold density below which the H-mode is never obtained for minimum P_{th} [6.5].

The dependence of $P_{th} / (\overline{n_e}^{0.5} B_t)$ on q_{eff} is shown in Fig. 6.7. For $q_{eff} < 7$ there is no q_{eff} dependence of P_{th}. However, the threshold power is found to increase with decreasing Ip for $q_{eff} > 7$. The q_{eff} dependence of $P_{th} / (B_t \overline{n_e}^{0.5})$ is written in the function of $g(q_{eff}) = \exp[\{(q_{eff}-1)/10\}^4]$. Therefore the following scaling is obtained; $P_{th}(MW) = 1.1 B_t(T) \overline{n_e}_{19}^{0.5} (10^{19}m^{-3}) f(\overline{n_e}) g(q_{eff})$. The comparison between the data and scaling of threshold power is shown in Fig. 6.8. There is good agreement between them.

Normalized P_{net} to P_{th} is shown in Fig. 6.9 for all data including high recycling shots. The values of P_{net} / P_{th} in the high recycling shots (shot no. < 23530) are large compared with that in the low recycling shots. Since recycling condition of the wall affects the threshold power, here the threshold power in only low recycling shots was discussed.

6.3 Discussion

The L-H transition threshold was studied using the net power reaching the plasma edge, $P_{net}^* = P_{net} - P_{rad}$ [6.6]. The value of P_{rad} is from 5 % to 20% of P_{net}. Even if the radiation is taken into account in the evaluation of P_{th}, the parametric dependence of P_{th} is the same as above-mentioned dependence and following scaling is obtained: $P_{th}(MW) = 1.0 B_t(T) \overline{n_e}_{19}^{0.5}(10^{19}m^{-3}) f(\overline{n_e}) g(q_{eff})$. Only factor is changed from 1.1 to 1.0.

6.4 Summary

The following scaling is obtained for $\overline{n_e}_{19} \leq 2.8$; $P_{th}(MW) = 1.1 B_t(T) \overline{n_e}_{19}^{0.5}(10^{19}m^{-3}) f(\overline{n_e}) g(q_{eff})$, where $f(n_e)$ is around unity for $\overline{n_e}_{19} \geq 1.2$ and $f = 1.2 / \overline{n_e}_{19}$ for $\overline{n_e}_{19} \leq 1.2$ and $g(q_{eff}) = \exp[\{(q_{eff}-1)/10\}^4]$. The density dependence of P_{th} was rather weaker than P_{th}^{ITER}. The threshold power increases with decreasing density in the range $\overline{n_e}_{19} \leq 1.2$. There is a threshold density below which the H-mode is never obtained for minimum P_{th}. For $q_{eff} < 7$ there is no q_{eff} dependence of P_{th}. However, for $q_{eff} > 7$ the threshold power decreases with increasing Ip.

References

[6.1] F. Riter *et al.*, in Controlled Fusion and Plasma Physics (20th EPS. Conf., Lisboa, 1993), Vol 17C Part I 15.

[6.2] P. N. Yushmanov *et al.*, Nucl. Fusion 30 (1990) 1999.

[6.3] M. Kikuchi *et al.*, in Plasma Physics and Controlled Nuclear Fusion Research (Int. Conf. Sevill,1994), IAEA-CN-60/AI-I-2.

[6.4] K. Tsuchiya *et al.*, section 8 in this report (1995).

[6.5] M. Sato *et al.*, in Plasma Physics and Controlled Nuclear Fusion Research (Int. Conf. Seville,1994), IAEA-CN-60/A2-II-4.

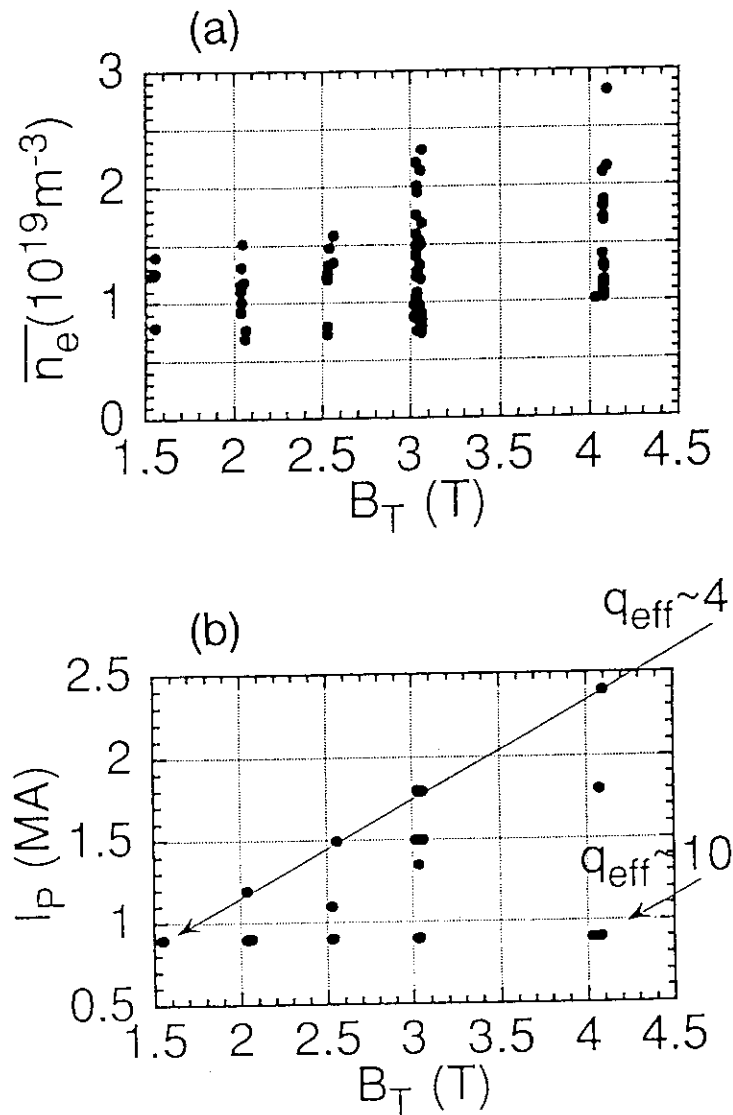[6.6] F. Riter *et al.*, Plasma Physics and Controlled Fusion 36 Suppl. (1994) A99.

Fig. 6.1 Discharge region. (a) $\overline{n_e}$ vs B_t (b) I_P vs B_t.
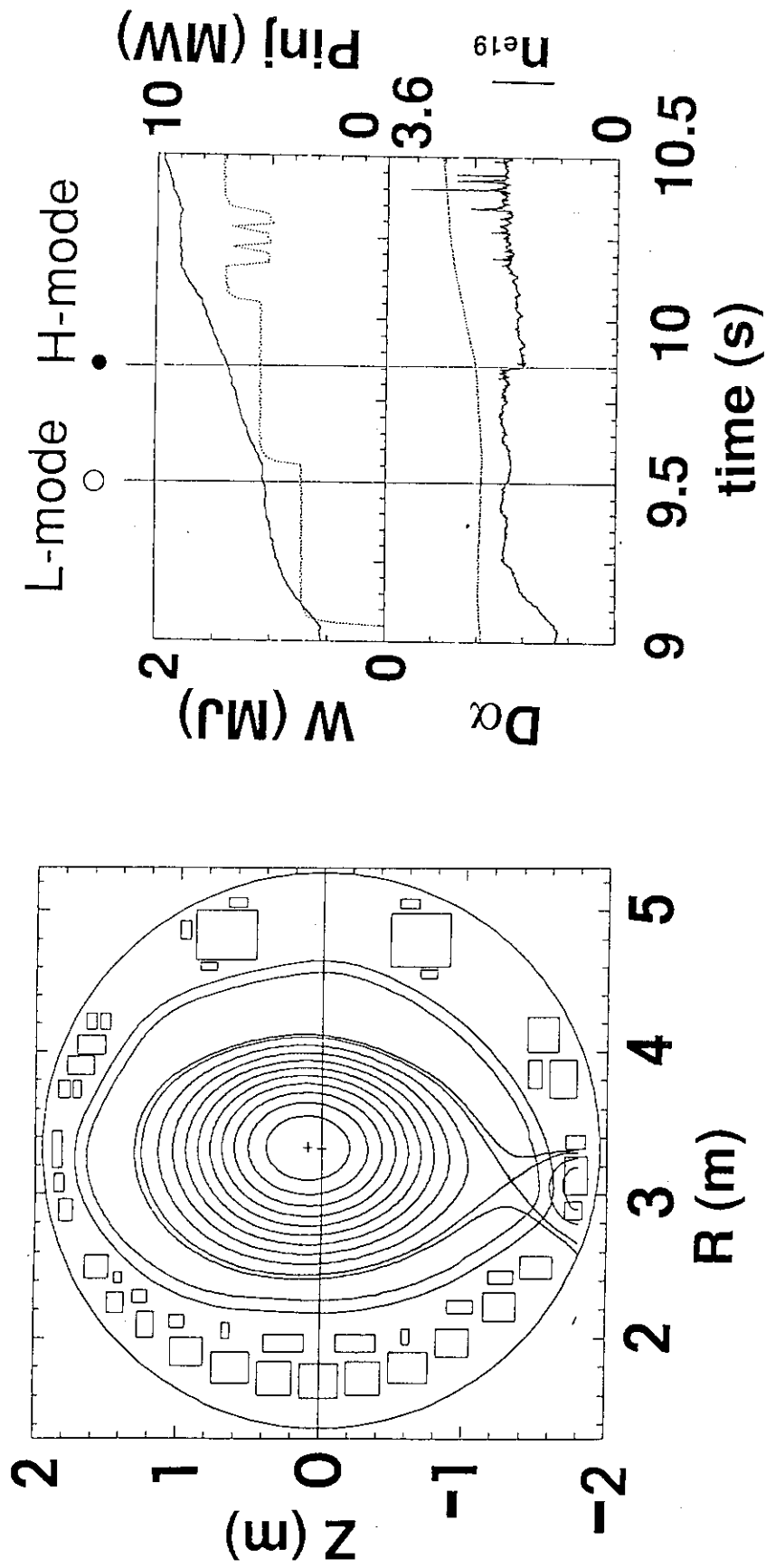
Fig. 6.3 Typical time evolution of plasma parameters.

Fig. 6.2 Typical configuration with small ripple-loss.
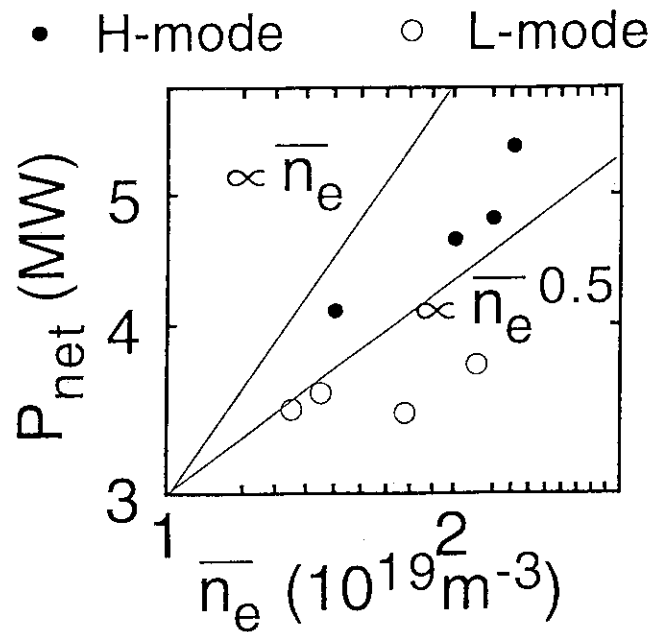
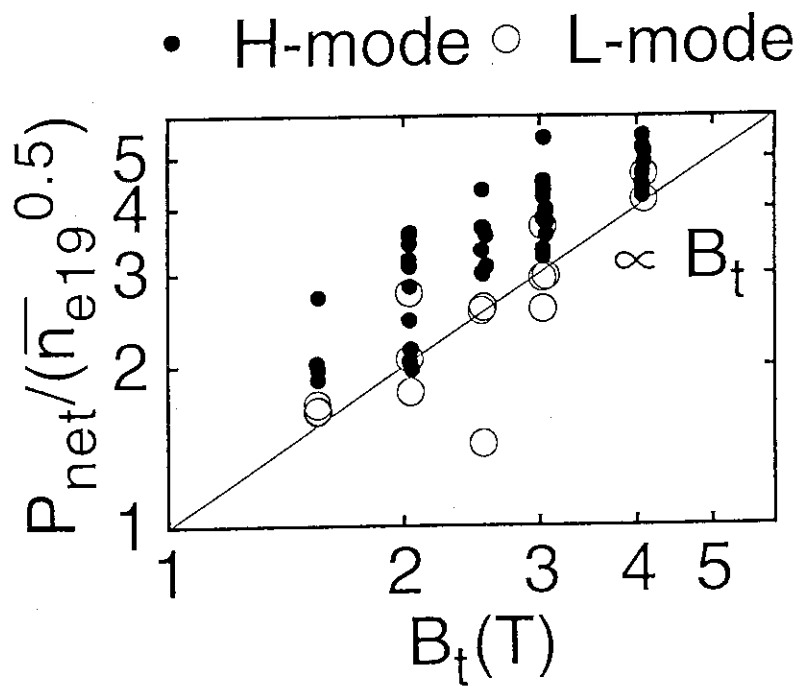Fig. 6.4 Density dependence of P_{th} for B_t =3T, Ip =1.8MA, $\bar{n}_{e19} \geq 1.2$.

Fig. 6.5 Toroidal magnetic field dependence of $P_{th} / \bar{n}_e^{0.5}$ for $\bar{n}_{e19} \geq 1.2$, $q_{eff} < 7$.

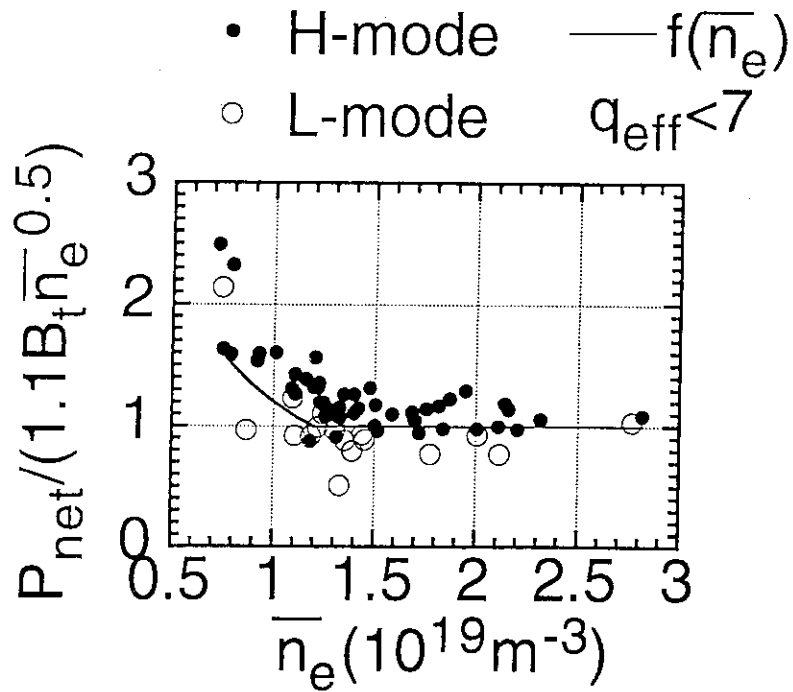**Fig. 6.6** Density dependence of $P_{th} / (\overline{n_e}^{0.5} B_t)$ including low density data for $q_{eff} < 7$.
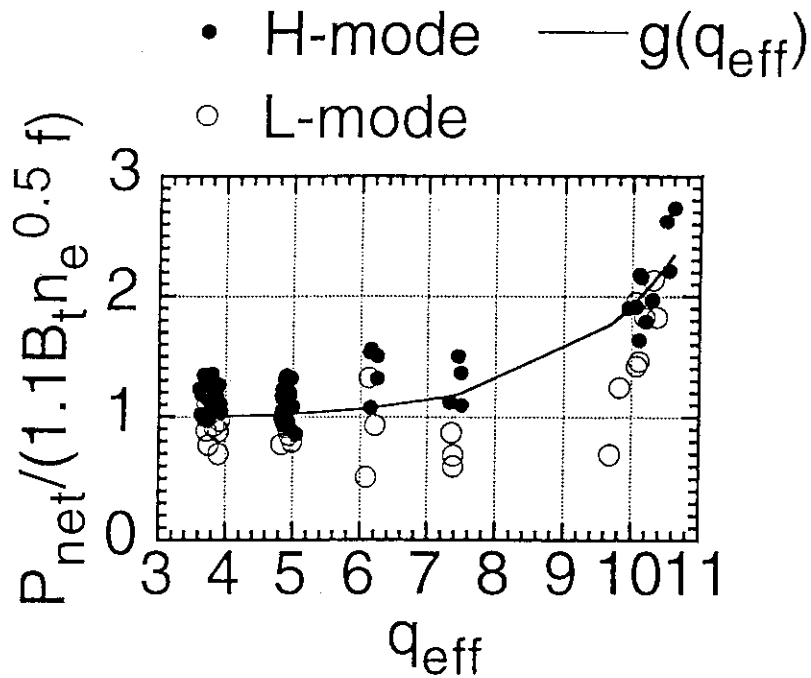
Fig. 6.7 In high q_{eff} region, the q_{eff} dependence of $P_{th} / (\overline{n_e}^{0.5} B_t)$ for $\overline{n_e}_{19} \geq 1.2$.
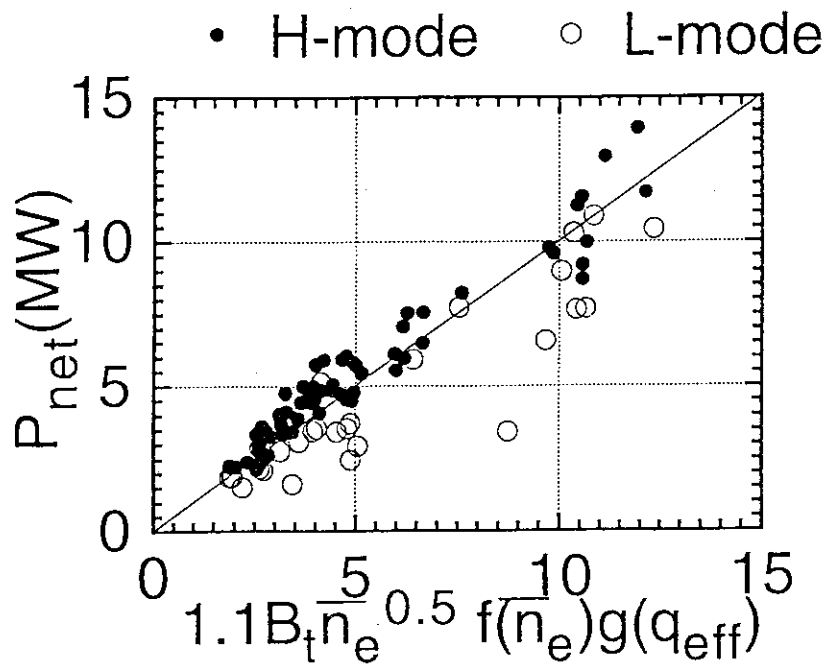
• H-mode   ○ L-mode

Fig. 6.8 Comparison between the all data except high recycling discharges and obtained scaling of threshold power.
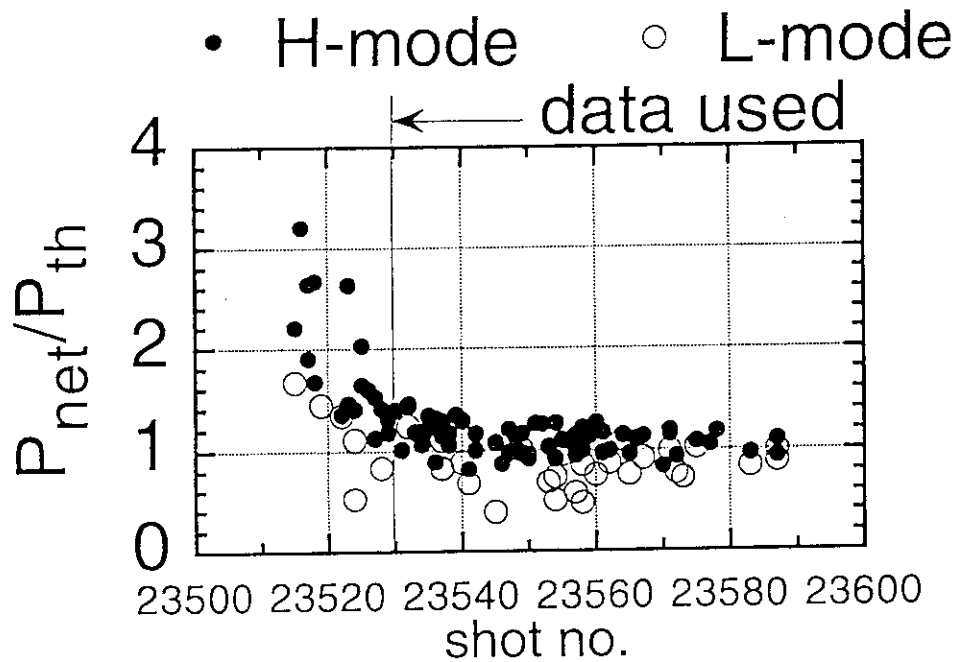
• H-mode   ○ L-mode

Fig. 6.9 Normalized P_{net} to P_{th} for all data including high recycling data.

7. Parametric Study of Edge Local Quantities across the H-mode Transition Observed at JT-60U

Takeshi FUKUDA, Masayasu SATO, Tomonori TAKIZUKA, Yutaka KAMADA,

Katsuhiko TSUCHIYA, Hidenobu TAKENAGA, Shinichi ISHIDA, Masahiro MORI

7.1 Introduction

It is now regarded to be inconceivable to operate fusion reactors without the H-mode, which is ubiquitously observed in various plasma devices. However, neither conditions to attain the H-mode nor physical mechanism has been fully understood. Therefore, it has been urged to compile the threshold database in order to predict the required heating capability in ITER, as well as to stimulate theoretical works.

Issues of investigations are (1) why the H-mode transition power threshold (P_{NB}^{th}) is remarkably dependent on B_T, but less significant on I_p, which is contrary to their contributions to the confinement properties, (2) whether the low density limit for the H-mode transition really exists and how it is scaled, (3) how much is the contributions of the neutrals on P_{NB}^{th}, (4) if the edge ion collisionality is an adequate criteria to describe the H-mode transition, (5) isotope effect, (6) how we can scale the L to H back transition and (7) whether the non-dimensional transition parameters can be an effective measure of P_{NB}^{th}. This paper mainly address the items from (1) through (5) except (3), of which detailed description is given in another section. Results of the scaling studies will also be briefly described, since it is discussed in the previous section.

7.2 Experiment

In order to reasonably reduce the influence of wall conditions as much as possible, power threshold data was obtained from the consecutive tokamak discharges in a single series of experiment. Neutral beam (NB) power was varied stepwise with the size of 1 - 2 MW during the discharge to effectively define the heating power right above and below the threshold. 118 H-mode transition data was obtained from 71 pulses, and the operational parameters were as follows: (a) I_p = 0.9 - 2.4 MA, (b) B_T = 1.5 - 4.0 T, (c) averaged density $\overline{n_e}$ = 0.7 - 2.8 x 10^{19} m^{-3}, (d) $V_p \sim$ 61.8 m^3 (S $\sim$ 138 m^2), (e) $X_p \sim$ 0.18 m and (f) $\kappa \sim$ 1.56. Averaged time derivative fraction of the stored energy $\dot{W}$, P_{rad} / P_{net} (= P_{abs} - $\dot{W}$ +P_{OH}) and the ripple loss (including the charge exchange and orbit loss) were respectively 22.0%, 13.1% and 24.3%. As we kept the equilibrium configuration the same throughout the experiment, the averaged Z_{eff} was 2.76, and the major impurity species were carbon ($\sim$ 3.5%) and oxygen ($\sim$ 1.6%).

Hereafter, carbon is regarded as an influential impurity species in the code analysis and the estimate of ion collisionality discussed in the later subsections.

In addition to the (i) increase of n_e and the diamagnetic stored energy W^{dia}, (ii) reduction of D_α and $\tilde{n_e}$ (with a multichannel microwave reflectometer) as well as the values of edge T_i and v_Φ, θ (with charge exchange recombination diagnostic of CVI line) were examined to determine the time of transition.

7.3 Threshold power scaling

NB absorption power and the ripple loss fraction were respectively evaluated by the TOPICS and OFMC codes, whilst ohmic input and the radiation power were obtained by the FBI code. As discussed in the prior section, P_{NB}^{th} is scaled as $n_e^{0.5} B_T^{1.0}$ in the region $\overline{n_e} \geq$ 1.5 x 10 ^{19} m $^{-3}$ [7.1]. This is congenial to the $ne^{0.75}B_TS$ scaling produced by the ITER H-mode database working group [7.2], which is weighted more on larger devices, and not to the $neB_TR^{0.75}$ scaling, seemingly due to the similar dependence on n_e. However, JT-60U's boundary is still 20% higher than the $ne^{0.75}B_TS$ scaling, in spite of the fact that the current data base for P_{NB}^{th} is the lowest, in comparison to the publications at IAEA Würzburg (1992) [7.3] and Seville (1994) [7.4] conference. Reduction in P_{NB}^{th} is believed to be ascribed to the way the database was compiled, and we suggest that the accumulation of the data taken at different occasions with even a slight difference of the equilibrium shape, may easily mislead the results of P_{NB}^{th} scaling. The quality of database having been remarkably improved, Ip dependence of P_{NB}^{th} was not resolved.

7.4 Relation between the threshold power scaling and local quantities

In this section, we will focus on the behaviour of P_{NB}^{th} in the low density regime, with respect to the edge local quantities. Among the various experimental documentations in various tokamaks, the significance of the edge plasma temperature has been disputed as one of the key issues to induce the H-mode transition. Theoretical considerations take this quantity in terms of the ion collisionality v_i^* ($= v_{ii}Rq/\varepsilon^{2/3}v_{th}$). As predicted by the Shaing's theory, high-energy collisionless particles contribute to the ion orbit loss and drive a poloidal torque, while low-energy collisional particles contribute to the poloidal viscosity and resist poloidal rotation. The critical v_i^* at which the poloidal flow velocity makes a sudden change to a more positive value is expected to be around unity. However, quantitative agreement with the theory has not been previously shown. A candidate for this discrepancy is the influence of impurities, since the transition condition must naturally be influenced by the impurities. One of the mechanism is the enhancement of the average ionic charge Z_{eff}. When Z_{eff} increases, pitch angle scattering of the bulk ions becomes more frequent and the threshold value increases. The other mechanism is

the non-ambipolar loss of impurities, which is caused by the rotation induced ion-ion collisions. JFT-2M evaluated at 7 mm inside the separatrix to obtain the value of v_i^* around 50, whereas for ASDEX it was larger than three. The DIII-D work also did not include the impurity effect.

In this work, we have investigated the effect of ion-impurity collision theoretically in terms of the normalized viscosity coefficient, considering the ion distribution function is non-Maxwellian in the area of our interest. Key impurity effect comes from the change of the deflection and the anisotropy relaxation frequencies by the impurity. In order to have the formula conserve the structure, we have replaced v_i^* with $v_i^* (Z_{eff} n_e / z_i^2 n_i)$ [7.5]. We can expect such an effect on fast ion orbit loss. This treatment is included hereafter for the estimate of the ion collisionality at the transition, and we denote as $v_i^*{}_{eff}{}^{95}$ evaluated at the 95% of the outermost flux surface position.

As seen in Fig. 7.1, $P_{NB}{}^{th}$ increases significantly in the region below $\overline{n_e} = 1.5 \times 10^{19}$ m^{-3}, whilst $v_i^*{}_{eff}{}^{95}$ is concomitantly reduced in the same region. Open circles indicate the data right before the transition, and crosses represent the data at the very end of the previous NB power step; namely right above and below $P_{NB}{}^{th}$, respectively. It is noteworthy as well that the value of ion collisionality was first shown to reside around unity in deuterium discharge in the region $\overline{n_e} \geq 1.5 \times 10^{19}$ m^{-3}. Slight decrease towards higher density region is also shown in Fig. 7.2, however, definitive statement will have to be done after obtaining additional transition data in the region $\overline{n_e} \geq 3.0 \times 10^{19}$ m^{-3}. Fig. 7.3 shows the relation between $T_i{}^{95}$ and $n_e{}^{95}$ for $\overline{n_e}$ over and below 1.2×10^{19} m^{-3}. Here, data was restricted to $q_{eff} (= q^{95}/0.95)$ < 8 from the reason mentioned in the succeeding paragraph. For $\overline{n_e} \geq 3.0 \times 10^{19}$ m^{-3}, $T_i{}^{95}$ increases as $n_e{}^{95}$, which supports the agreement with the constant collisionality. However, in the region $\overline{n_e} \geq 3.0 \times 10^{19}$ m^{-3}, $T_i{}^{95}$ soars in the fixed $n_e{}^{95}$ region. This result indicates that the reduction of $v_i^*{}_{eff}{}^{95}$ is ascribed to the increase of $T_i{}^{95}$ i.e., additional NB power is necessary to increase $T_i{}^{95}$ and make $v_i^*{}_{eff}{}^{95}$ reach the value as low as adequate for transition in the low density regime. The role of neutral density n_0 to reduce the threshold of $v_i^*{}_{eff}{}^{95}$ is discussed in the succeeding section, where it is documented with the use of DEGAS code that an increase of $n_0{}^{95}/n_e{}^{95}$ can cause the reduction of threshold value of $v_i^*{}_{eff}{}^{95}$ [7.6]. We also know from the previous experimental results that beam deposition profile is more peaked for low density target plasmas. Therefore, edge heating is less effective for low density plasmas, and it is possible that the necessary NB power is even more enhanced to induce the transition.

As we have observed peculiar feature for the data $q_{eff} > 8$, we have divided the low density data $\overline{n_e} \leq 1.5 \times 10^{19}$ m^{-3} into three regions of (1) $3.6 < q_{eff} < 4.0$, (2) $4.3 < q_{eff} < 7.7$ and (3) $9.1 < q_{eff} < 11$. As seen in Fig. 7.4, apparent q_{eff} dependence on the low density limit was resolved. Although the difference between the cases of (1) and (2) is subtle, it is shown that larger q_{eff} can increase the low-density transition boundary significantly. From the

assumption that the width of scrape-off-layer (SOL) λ_c, which is directly relevant to the penetration of neutral particles, is proportional to $(2D_\perp L_c/C_s)^{1/2}$ [7.7], where C_s, L_c and $D_\perp$ are respectively ion acoustic velocity $(= \{k(T_e+T_i)/m_i\}^{1/2})$, connection length $(= qR)$ and Bohm diffusivity $(= 0.06 T_e$ (eV) $/B_T$(T)), one might expect that edge neutral density has a definitive role to define the low density transition limit. However, λ_c can also be reduced to $T_e^{1/4} I_p^{-1/2} = I_p^{-1/4}$ (supposing $T_e^{95} \propto I_p$), which again defies the inclusion of B_T in the P_{NB}^{th} scaling. Having an equation that the penetration depth is described as $\lambda_{iz} \propto \overline{n_e}^{-7/10} \sim I_p^{-7/10}$ (assuming $n_e^{95} \propto I_p$) in mind, it has to be further investigated why the I_p dependence was not apparently seen. In addition, the role of neutrals in regard to the origin of density dependence will be another issue of further studies. DEGAS analysis would have to be extended to higher density region to show that neutral density increase with the density.

Boundaries of P_{NB}^{th} in each q_{eff} regime was fitted with the function; iz. $f(\overline{n_e}, q_{eff}) = a + b/(\overline{n_e} + c)^d$, and P_{NB}^{th} data was divided by the relevant $f(\overline{n_e}, q_{eff})$, which provided the Fig. 7.5. It shows that the whole data, regardless of the ranges of $\overline{n_e}$ and q_{eff}, can be fitted to the $n_e^{0.5} B_T^{1.0}$ scaling. However, it is noteworthy that for the first 10 to 20 discharges, there exist several data, which is well above P_{NB}^{th}. These data shows higher T_i^{95} for n_e^{95}, in comparison to other data obtained in the later phase of the experiment, which is indicative of the influence of wall conditions (either impurity or neutrals).

In many of the discharges sawteeth were present. However, it was observed that under the heating power defined as right below P_{NB}^{th}, plasma did not turn into the H-mode, until the NB power step was increased. This result indicates that the amount of heat flux emitted from the core region of the plasma and passes through the edge layer is less than the NB power step.

Inclusion of the radiation loss from the main plasma region did not remarkably modify the scaling established. Its influence, which indicates the $n_e^{\alpha(Zeff)}$ dependence was not observed, due to the relatively small fraction P_{rad}/P_{net} of 13.1%. As to the ripple loss effect, which is scaled as $n_e^{0.53} I_p^{-0.04}$ for a fixed configuration, neither exhibited major modifications to the scaling, and it only reduced the coefficient from 1.0 to 0.63. It was also found that P_{NB}^{th} data with the inclusion of the radiation power and ripple loss agreed well (absolute values were also similar) with the $n_e^{0.75} B_T S$ scaling produced by the ITER H-mode database working group.

7.5 Addendum

This subsection mainly deals with the P_{NB}^{th} data obtained in the last experimental campaign, where comparison of the threshold power and edge local parameters were compared between the deuterium and hydrogen discharges, as well as the grad-B direction towards and against the X-point. The equilibrium configuration was very similar to the one recently analyzed, and the operational parameters were: (a) $I_p = 0.95 - 1.72$ MA and (b) $B_T = 2 - 3.5$ T.

Since the comparison of the absolute value of P_{NB}^{th} with the recent experiment is believed to be difficult, result of relative comparison is summarized in this paper. P_{NB}^{th} is the largest for the case ∇B drift direction against the X-point with deuterium as an acting gas, and larger for hydrogen discharge with ∇B drift direction towards the X-point. The smallest was the deuterium with ∇B drift direction towards the X-point. Recalling that deuterium reduces the edge transport by the mass effect, it can be speculated that P_{NB}^{th} is smaller when edge confinement is improved. Superior transport property makes it easier to increase the edge ion temperature i.e., to reduce the value of $v_i^{*}{}_{eff}$. Compiled data was smaller than the expectations from the $1.5B_T^{1.5}$ scaling, and the density dependence was not clearly resolved in this experimental campaign. It has to be mentioned that the number of pulses undertaken for this particular experiment was less than the recent experiment.

The value of $v_i^{*}{}_{eff}$ was the same between the deuterium and hydrogen discharges. This is reasonable, since root-squared mass terms included in the numerator and denominator cancel out in the v_i^{*} formula. When the direction of B_T was reversed, however, the value of $v_i^{*}{}_{eff}$ was reduced, as in the case of the low density discharge mentioned in the previous subsections. Since the value of $v_i^{*}{}_{eff}$ at the transition is not influenced by the changes of equilibrium configuration, this result might be indicating the changes of edge neutral density. This is also consistent with the fact that P_{NB}^{th} was the largest for the case of ∇B drift direction against the X-point. In addition, q_{eff} dependence was not found in this campaign. Comparison of the edge T_i and T_e showed similar tendency to the recent experiment.

7.6 Discussion

Although the quality of the transition database was remarkably improved, further investigations to understand the influence of neutrals as well as the reason why the contribution of Ip is not apparent would have to be pursued.

7.7 Summary

In order to reasonably reduce the influence of wall conditions as much as possible, power threshold data was obtained from the consecutive tokamak discharges in a single series of experiment with a fixed equilibrium configuration. P_{NB}^{th} is scaled as $n_e^{0.5} B_T^{1.0}$ in the region $\overline{n_e} \geq 1.5 \times 10^{19}$ m^{-3}. This is congenial to the $n_e^{0.75}B_T S$ scaling produced by the ITER H-mode database working group. Thus, the quality of database having been remarkably improved, Ip dependence of P_{NB}^{th} was not resolved.

We have clearly documented that the low density limit for the H-mode transition does exit, and it can be scaled with q_{eff} or the edge neutral density. Therefore, it was suggested that the density limit can be machine dependent. We have also shown that increase of the edge

neutral density reduces the value of ion collisionality required to induce the transition, which significantly increase the necessary NB heating power. Above results makes us deduce that the ion collisionality is not the sole necessary condition for the H-mode transition, and we are urged to seek for the full set of criteria.

Acknowledgments

One of the authors (TF) is grateful to Dr. K. Shaing for the stimulating discussions.

References

[7.1] M. Sato *et al.*, section 6 in this report (1995).

[7.2] H-mode Database Working Group, Proc. 21st EPS Conf., Vol. I (1994) 334.

[7.3] M. Kikuchi *et al.*, Proc. 14th Int. Conf. on Plasma Physics and Controlled Nuclear Fusion Research, Vol.I (1992) 189.

[7.4] M. Sato *et al.*, Proc. 15th Int. Conf. on Plasma Physics and Controlled Nuclear Fusion Research, IAEA-CN-60/A-2-II-4 (1994).

[7.5] T. Fukuda *et al.*, Plasma Physics and Controlled Fusion **36**-(7)A (1994) A87.

[7.6] K. Tsuchiya *et al.*, section 8 in this report (1995).

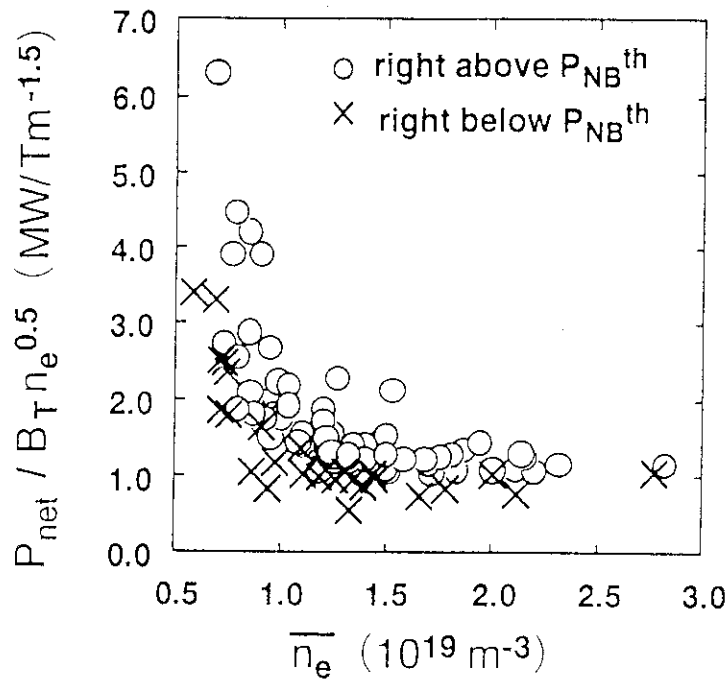[7.7] P.C.Stangeby *et al.*, Nucl. Fusion **30** (1990)1225.

Fig. 7.1 Relation between $P_{net}/B_T n_e^{0.5}$ and $\overline{n_e}$. P_{NB}^{th} increases significantly in the region below $\overline{n_e} = 1.5 \times 10^{19}$ m^{-3}. Circles indicate the data right before the transition, and crosses represent the data at the very end of the previous NB power step; namely right above and below P_{NB}^{th}, respectively.
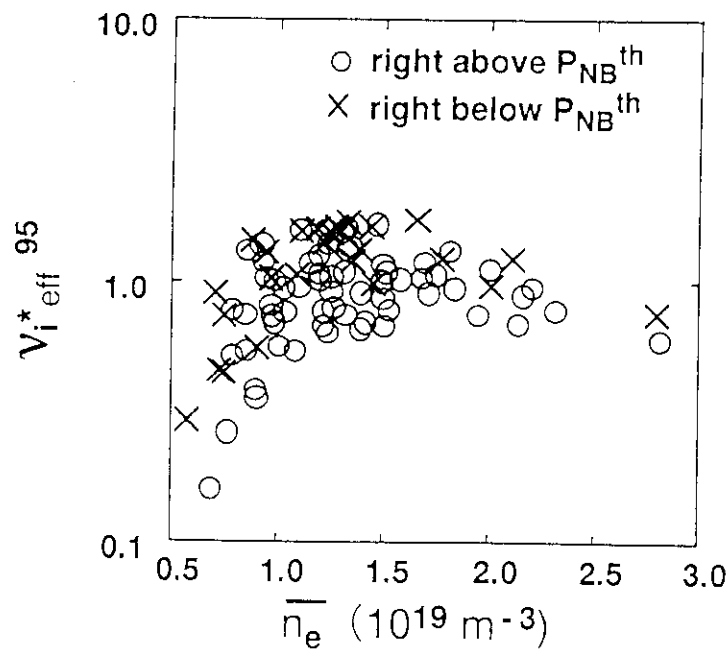

Fig. 7.2 Relation between $v_i^{*}{}_{eff}^{95}$ and $\overline{n_e}$. $v_i^{*}{}_{eff}^{95}$ is concomitantly reduced in the region below $\overline{n_e} = 1.5 \times 10^{19}$ m^{-3}. Symbols are the same as in Fig. 7.1.
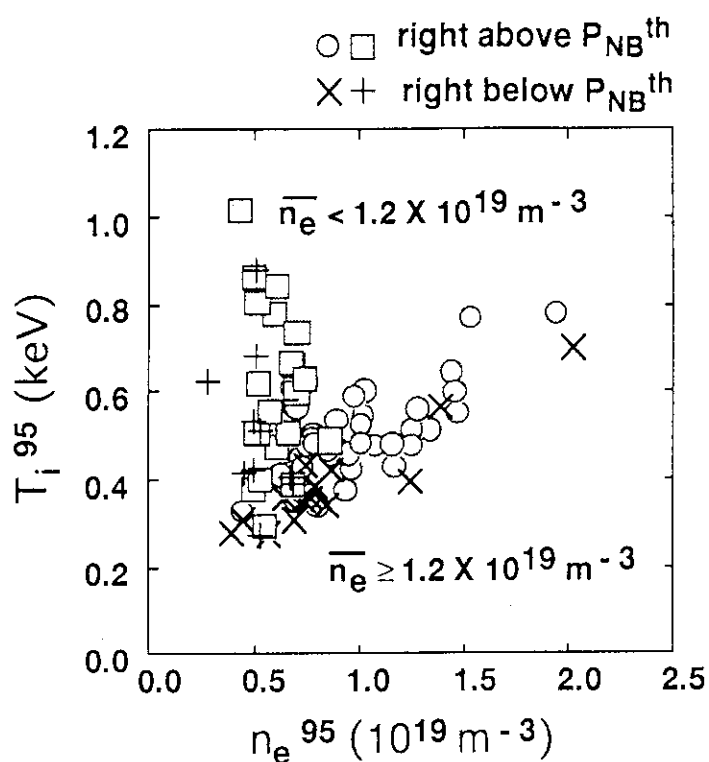
Fig. 7.3 Relation between $T_i{}^{95}$ and $n_e{}^{95}$ for $\overline{n_e}$ over and below 1.2×10^{19} m^{-3}. Here, data were restricted to q_{eff} ($= q^{95}/0.95$) < 8.
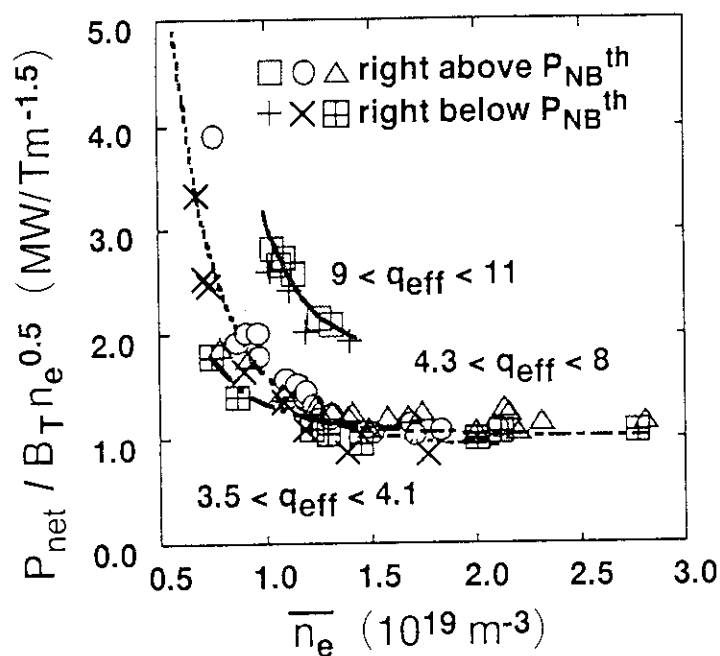

Fig. 7.4 Relation between $P_{net}/B_T n_e{}^{0.5}$ and $\overline{n_e}$ for various q_{eff} values; (1) $3.6 < q_{eff} < 4.0$, (2) $4.3 < q_{eff} < 7.7$ and (3) $9.1 < q_{eff} < 11$.
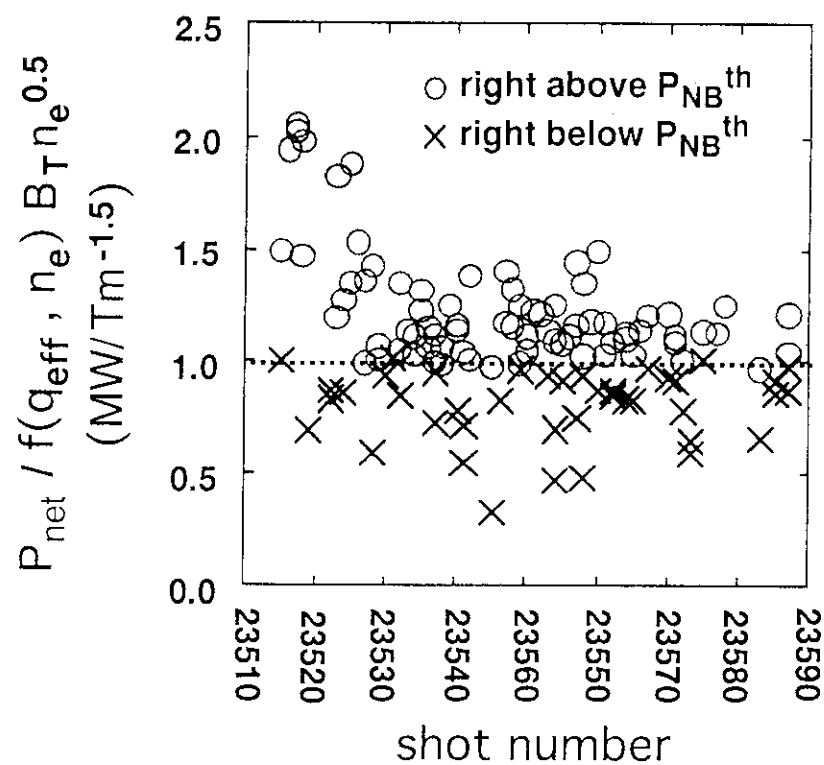
Fig. 7.5 Boundaries of P_{net} devided by $B_T n_e^{0.5} f(\overline{n_e}, q_{eff})$. The whole data, regardless of the ranges of $\overline{n_e}$ and q_{eff}, are fitted by the $n_e^{0.5} B_T^{1.0}$ scaling.

8. Effect of Edge Neutrals on the Condition of H-mode Transition in JT-60U

Katsuhiko TSUCHIYA, Hidenobu TAKENAGA, Takeshi FUKUDA, Yutaka KAMADA,

Shinichi ISHIDA, Masayasu SATO, Tomonori TAKIZUKA

8.1 Introduction

H-mode transition in JT-60U was intensively investigated for the understandings of mutual relationship between the global parameters; such as the net heating power, electron density, plasma current and toroidal field strength, and the edge local quantity, as represented by the ion collisionality. The features of H-mode transition were mainly studied in the past in terms of the effective edge ion collisionality ($v_i^*{}_{eff}$), where the impurity effect was included [8.1]. It is theoretically suggested by Shaing and Crume [8.2] that this quantity is related to the orbit excursion of edge ions which induces the radial electric field E_r, and the H-mode transition takes place under the condition that v_i^* is around unity.

It has been found in JT-60U, however, that the L-mode phase can persist even at $v_i^*{}_{eff}$ much less than unity. This phenomena was often observed when the intensity of D_α line and the amount of charge-exchange neutral flux were relatively large. Therefore, we have speculated that the edge neutrals affect the criteria of H-mode transition, and calculated the neutral particle density near the separatrix by using the DEGAS code [8.3]. Influence of the neutral particles on the transition criteria has also been disputed as an urgent issue of investigation in the ITER physics R&D tasks.

Experiments for the detailed investigation of H-mode transition power threshold were recently carried out [8.4], in a way that repetitive tokamak pulses were produced with fixed equilibrium configuration, and only the plasma current, toroidal magnetic field and the electron density were varied. Analysis of the neutral density was carried out on the database obtained in the series of experiments described above.

8.2 The estimation method of edge neutral density

The edge neutral density is estimated by the Monte-Carlo code DEGAS. The flow chart of calculation is shown in Fig. 8.1. The plasma equilibrium configuration was calculated with the FBEQU code, and its output parameters were used in DEGAS. Edge plasma parameters, were calculated with the two-dimensional divertor code based on a simple model [8.5], to which we apply the measured data by Langmuir probe array on the divertor plates. The

absolute value of neutral density was adjusted to be consistent with the Dα intensity. The lines of sight for this measurement are shown in Fig. 8.2. Averaging the calculated density over the poloidal direction on the surface of r/a = constant, n_0(r/a) was evaluated. The edge neutral density (n_0^{95}) used hereafter is defined by averaging n_0(r/a) from r/a=0.95 to 1.0 (i.e. LCFS), in order to reduce the Monte Carlo calculation noise.

8.3 Results and discussion

Database for the threshold power experiments consists of discharges with I_p=0.9-2.4 MA and B_T=1.5-4.0 T [8.4]. Figure 8.3 shows the waveforms of a typical discharge included in the analysis database. H-mode transition occurs at t = 8.17 sec in this particular pulse. During the series of these experiments, the plasma configuration was kep fixed, and the injection NB power was varied stepwise in time. Figure 8.4 shows the averaged electron density (n_e^{av}) dependence of $v_i^*{}_{eff}$ which is defined as $v_i^*{}_{eff}=(n_e Z_{eff}/n_i Z_i^2)(v_{ii} qR/\varepsilon^{3/2} v_{th})$. The ion collision frequency is $v_{ii} = 16 \backslash r(\pi) n_i e^4 \ln\Lambda Z_i^4/3 \backslash r(m)(2T)^{3/2}$, and the ion thermal speed is $v_{th} = \backslash r(2T/m)$, where m and T are ion mass and ion temperature, respectively. ε is the inverse aspect ratio (= a/R). Z_i is the charge number of impurity which is assumed to be 6. The circles indicate the data right before H-transition, and the crosses are for the one NB power-step prior to the H-mode transition. The n_e^{av} dependence of $v_i^*{}_{eff}$ is constant in the case of $n_e^{av} > 1.2 \times 10^{19}$ m^{-3}. Under the condition of low density (less than 1.2×10^{19} m^{-3}), $v_i^*{}_{eff}$ shows the significant descrease in regard to the plasma density. This dependence indicates that decrease of the density is directly related to the deteriorated accesibility to the H-mode. In this case, the heating power to attain the H-mode significantly soared. Therefore, the edge ion temperature right before the transition was considerably larger than the case of $n_e > 1.2 \times 10^{19}$ m^{-3}, which is consistent with the reduced edge ion collisionality [8.4]. Figure 8.5 shows the dependence of n_0^{95} on n_e^{95} for a part of data shown in Fig. 8.4. n_e^{95} stands for the electron density at r/a = 0.95. The n_e^{95} dependence of n_0^{95} was not clear. However, it is noteworthy that the values of n_0^{95} at the beginning phase of the series of experiment are larger than the others at the same value of n_e^{95}. This is also consistent with the experimental evidence that the threshold power for the H-mode transition gradually decreases as the first wall is conditioned with the repetitive tokamak discharges [8.4].

Figure 8.6 shows the correlation of $v_i^*{}_{eff}$ and n_0^{95}/n_e^{95} for the same data as Fig. 8.5. It can be seen that $v_i^*{}_{eff}$ at the transition tends to decrease with the increase of n_0^{95}/n_e^{95}. In addition, both L- and H-mode phases are clearly separated on this plane. Therefore, the edge neutral density affects the increase of threshold power in the range of low density. The edge neutrals have a key role of the condition of H-transition.

8.4 Summary

Effect of neutral density on the H-mode transition was experimentally studied in JT-60U. The neutral density near the separatrix was evaluated with the DEGAS code. We have obtained the result which indicates strong correlation between v_i^*eff and n_o^{95}/n_e^{95}. This means that the edge neutrals have a substantial influence on the condition of H-mode transition in the low density plasmas.

Acknowledgement

References

[8.1] T. Fukuda *et al* ., Plasma Phys. and Control. Fusion **36** (1994) A87.

[8.2] K.C. Shaing and E.C. Crume, Jr., Phys. Rev. Lett. **63** (1989) 2369.

[8.3] D.B. Heifetz *et al.* , J. Compt. Phys. **46** (1982) 309.

[8.4] M. Sato *et al.*, section 6 in this report (1995).

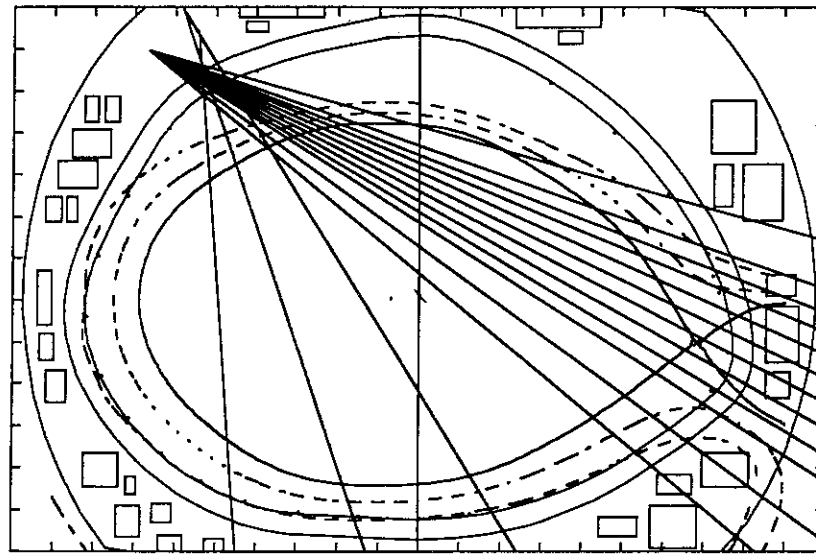[8.5] K. Shimizu *et al.*, J. Nucl. Mater. **196-198** (1992) 476.
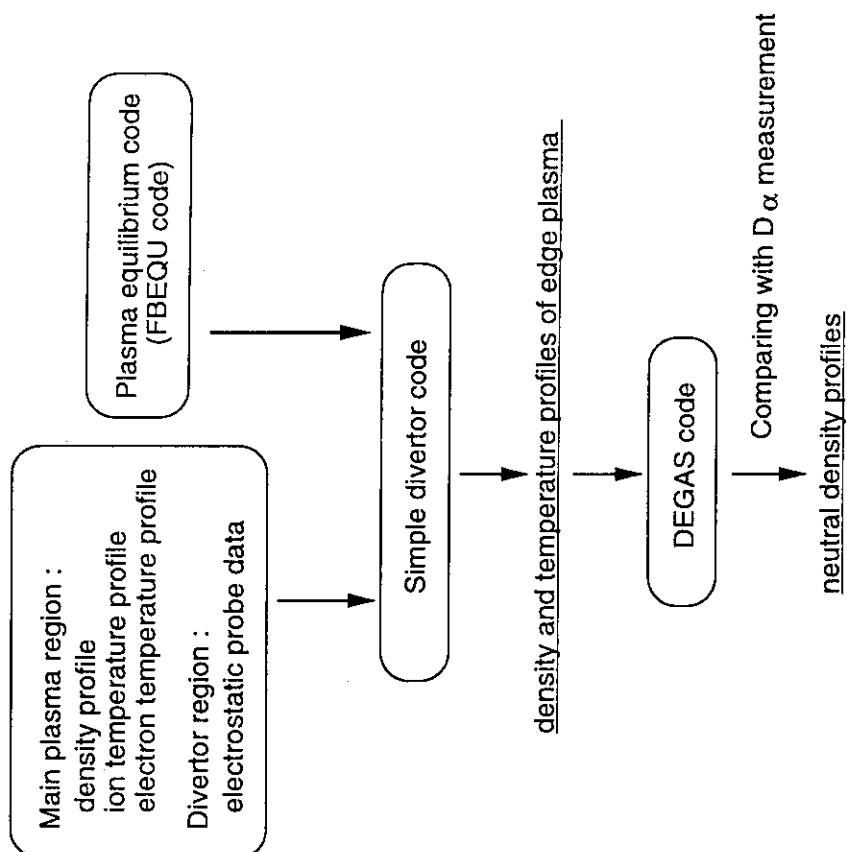
Fig. 8.2 Lines of sights for Dα measurement.
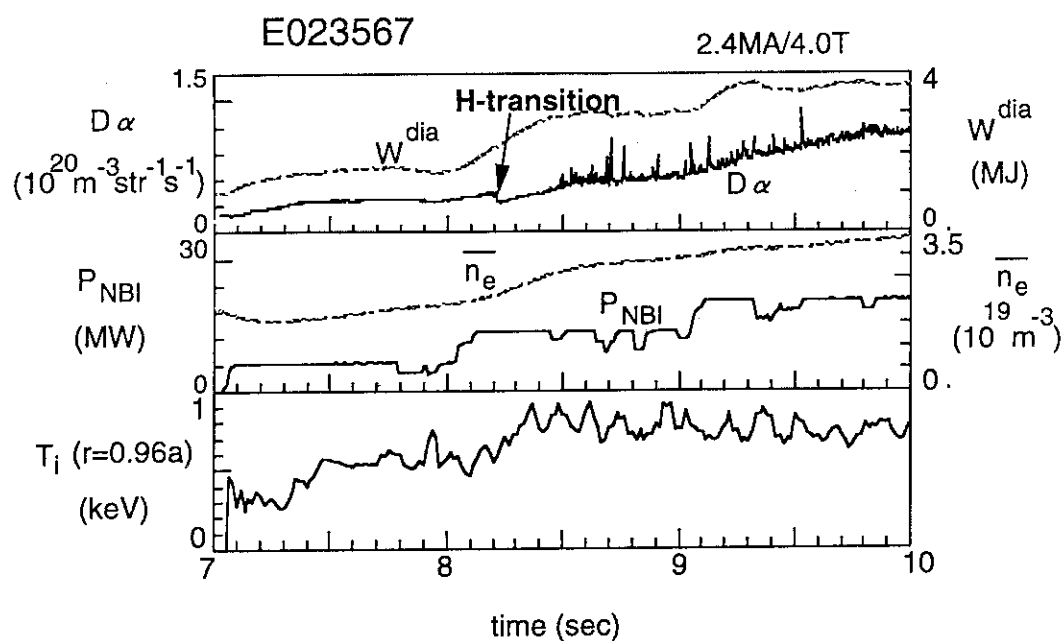

Fig. 8.1 Flow chart of the neutral density calculation.

Fig. 8.3 Traces of a typical shot on the discharge with I_p = 2.4MA and B_T = 4.0T.

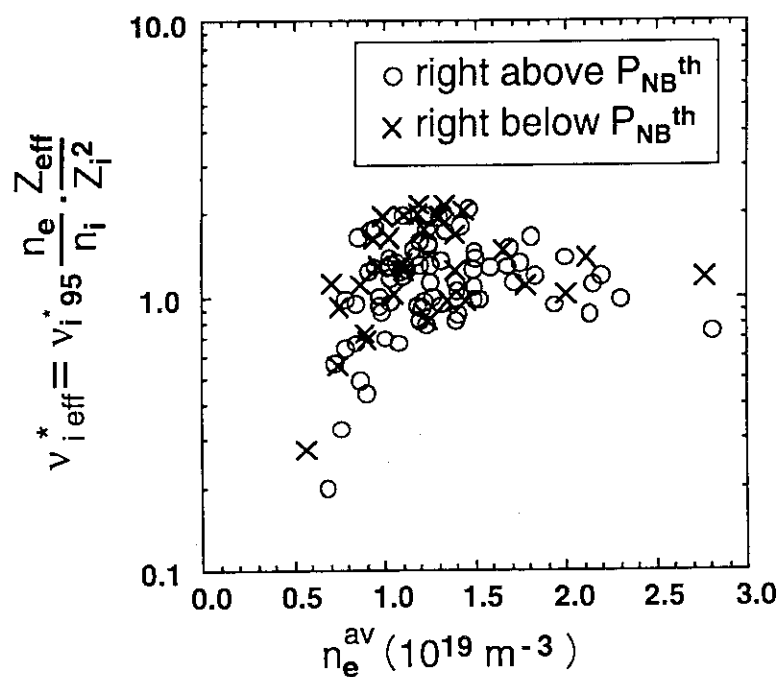Fig. 8.4 Electron density dependence of $v_i{}^*{}_{eff}$ for the data of discharges with I_p = 0.9-2.4MA and B_T = 1.5-4.0T.
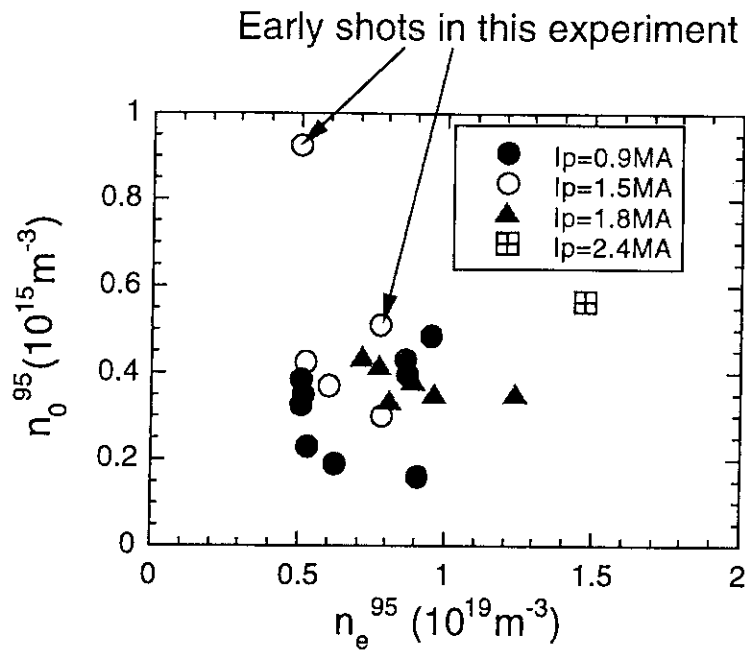
Early shots in this experiment

Fig.8.5 Dependence of $n_0{}^{95}$ on $n_e{}^{95}$ for a part of the same data as Fig. 8.4.
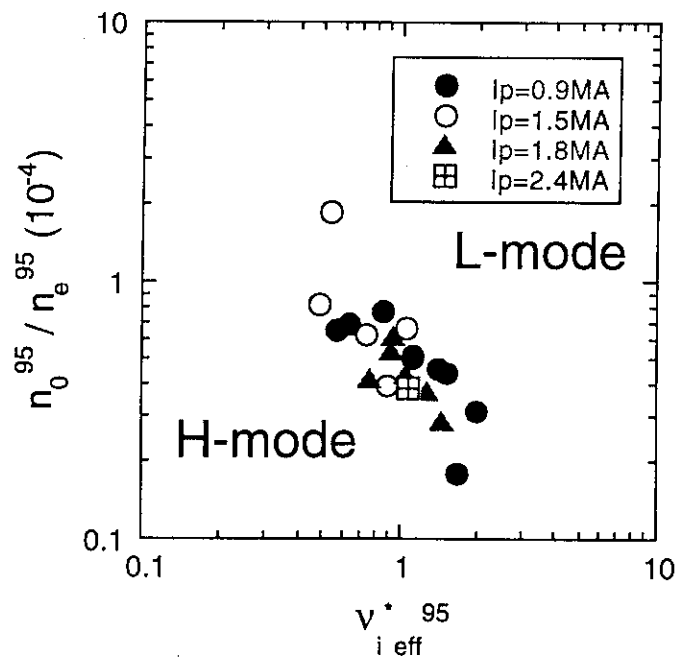

Fig. 8.6 Correlation of $\nu_i{}^*{}_{eff}$ and $n_0{}^{95}/n_e{}^{95}$ for the same data as Fig. 8.5.

9. H-L Back Transition in JT-60U

Hidenobu TAKENAGA, Takeshi FUKUDA, Yutaka KAMADA, Katsuhiko TSUCHIYA

Back transition phenomenon from H-mode to L-mode is crucial for understanding physical mechanisms improving confinement properties and operating regimes of H-mode plasmas. Thus, it is an urgent task for ITER R&D to establish a data base of the threshold power for the H-L back transition. In JT-60U, the H-L back transition was observed in the several cases, and here, we discussed the properties of three typical H-L back transitions. These occurred 1) after the end of the NB heating phase (case 1), 2) during the density increasing phase due to strong gas-puffing (case 2) and 3) when the wall conditioning was insufficient (case 3), which is related to the high recycling factor and/or a large amount of the impurities generation at the first wall and the divertor plates.

Figure 9.1 shows typical time traces for case 1 of averaged electron density (n_e), stored energy (W_{dia}), NB input power (P_{NBI}) and D_a emission intensity observed using a chord viewing the divertor region. In this discharge, plasma current (I_p) was 0.9MA, magnetic field (B_T) was 2T and NB heating was applied during t=8.6-10.1s. Violent ELM activity appeared at t=8.9s, and continued until t=10.3s although the NB heating phase had been terminated at t=10.1s. The H-L back transition occurred at 200ms after the end of the NB heating phase. In the NB heating phase, the energy confinement time was estimated to be 160ms at t=9.8s. The delay time of the H-L back transition from the end of the NB heating phase was comparable to the energy confinement time. This delay time might be thought to correspond to the decay time of the ion temperature at the plasma edge, because the energy confinement time decide the decay time of the edge ion temperature when the NB heating power depositing in the central region was terminated. It has been reported that the edge ion temperature is a key parameter for the L-H transition [9.1], and also, above results suggest that the edge ion temperature plays an important role for the H-L back transition.

In Fig. 9.2, typical time traces for case 2 (I_p=1.2MA, B_T=2T) of n_e, W_{dia}, P_{NBI}, amount of gas-puffing and D_a emission intensity were shown. In this discharge, the amount of gas-puffing was controlled with a feed back algorithm using the measured average electron density. It is noted that D_a emission intensity in this discharge was much larger than that in the other two discharges. ELM activity started just after main NB heating was applied and gas-puffing was applied during t=8.9-10s. The value of ne and the base intensity of the D_a emission increased with the amount of gas-puffing and ELM became inactive gradually during t=9.0-9.2s. Then, ELM disappears and ne was kept constant in spite of increasing of the amount of gas-puffing, in contrast, D_a emission intensity increased. The enhancement factor

over the ITER-89P L-mode scaling decreased from 1.3 at t=8.6s to 0.95 at t=9.6s. These results indicate the occurrence of the L-H back transition, however, it can be seen from Fig. 9.2 that this case does not have a clear H-L back transition. The theory was proposed where the transition becomes a soft type transition under the high neutral particle density condition [9.2]. This case is consistent with this theory, because the neutral particle density had to be high due to the strong gas-puffing as shown by the large intensity of D_a emission.

Figure 9.3 shows typical time traces for case 3 (I_p=1.5MA, B_T=2.5T) of n_e, W_{dia}, P_{NBI} and D_a emission intensity. In this case, the L-H transition and the H-L back transition occurred repeatedly. As described before, this case was usually observed when wall conditioning was insufficient, which is related to the high recycling factor and a large amount of impurities generation. Therefore, these phenomena were discussed from the viewpoint of the change of the effective ion collisionality including the effect of impurities and the change of the neutral particle density [9.3].

In the present work, the study of the H-L back transition was limited qualitatively. In order to identify the mechanisms which decide the condition of the H-L back transition, it is necessary to accumulate a data base of the parameters influencing the transition such as NB heating power, the edge ion temperature and the neutral particle density, quantitatively.

References

[9.1] M. Kikuchi *et al.*, in Controlled Fusion and Plasma Physics (Proc. 20th Eur. Conf., Lisboa, 1993) Part I (1993) I-179.

[9.2] S.-I. Itoh and K. Itoh, Nucl. Fusion 29 (1989) 1031.

[9.3] K. Tsuchiya *et al.*, "Effect of Edge Neutrals on the Condition of H-mode Transition in JT-60U", section 8 in this report.
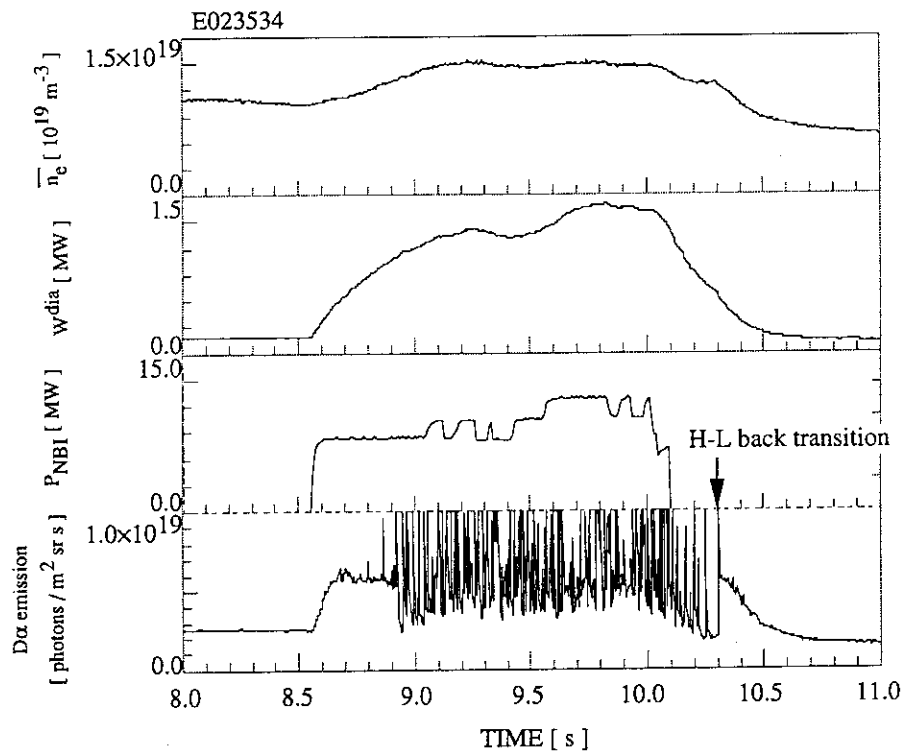
E023534
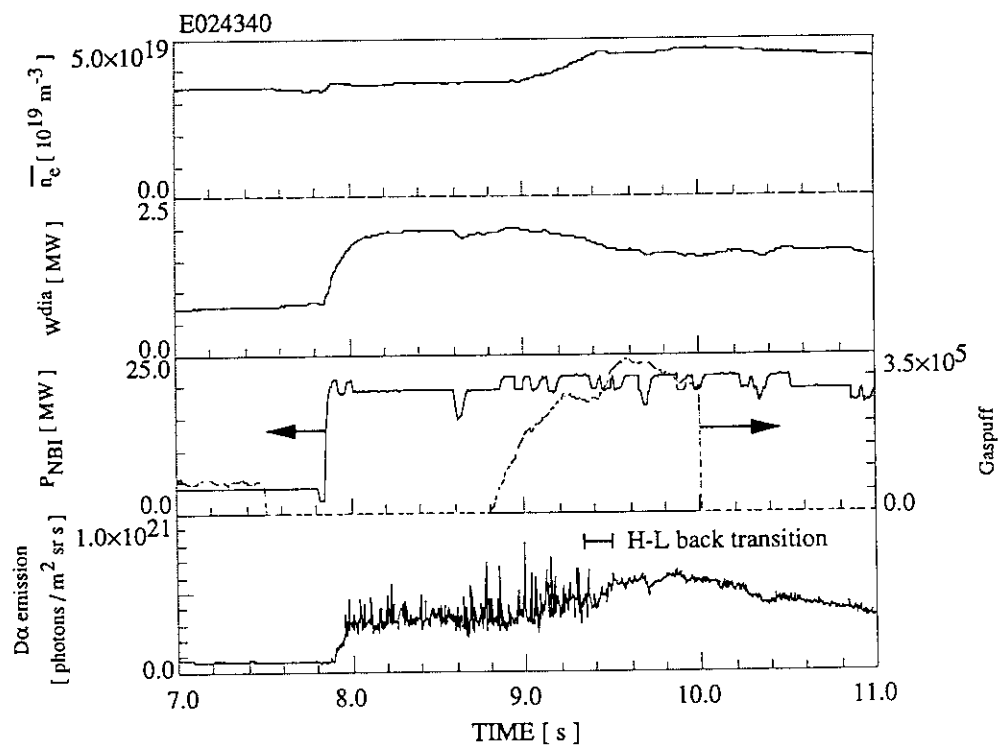

Fig. 9.1 Typical time traces for case 1
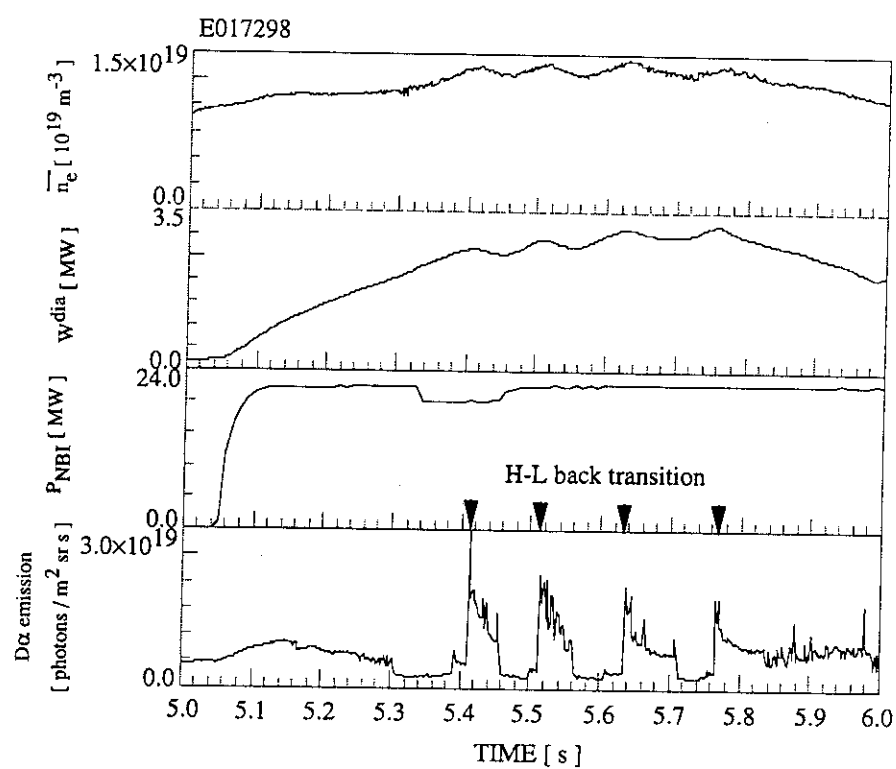
E024340

Fig. 9.2 Typical time traces for case 2

Fig. 9.3 Typical time traces for case 3

10. Onset Condition of ELMs in JT-60U

Yutaka KAMADA, Ryuji YOSHINO, Yuzuru NEYATANI, Masayasu SATO,

Shinji TOKUDA, Masafumi AZUMI, Satoru TAKEJI, Kenkichi USHIGUSA,

Takeshi FUKUDA, Masahiro MORI, Tomonori TAKIZUKA

10.1 Introduction

The ELMy H-mode is the candidate for the steady-state operational mode in the tokamak fusion reactors. Therefore control of the ELM behavior is one of the most important issues in sustainment of the highly integrated plasma performance. There are three types of ELMs observed in JT-60U (see below), out of which this paper concentrates on the giant ELMs. This is because appearance of the giant ELMs limits the achievable edge density and pressure and also tends to restrict the core plasma performance through the profile effects on stability and transport. For H-mode plasmas with broad pressure profiles, the edge pressure limit directly determines the global β_N limit [10.1]. The edge pressure limit also affects the ELM frequency f_{ELM}: The low pressure limit increases f_{ELM} at a given heating power and results in poor confinement in a ELMing steady-state. To contribute to establish the control scenario of the ELM behaviors, this paper identifies the onset conditions of the giant ELMs and emphasizes the effects of plasma shape such as triangularity δ and elongation κ.

For the typical shapes of JT-60U plasmas with $\delta \sim 0.1$, two types of ELMs have been observed. The first is the dithering ELM, which appears when the heating power P_{net} is around the threshold power for the L-H transition. The second is the giant ELM observed when the edge pressure reaches a critical value. When both δ and β_p are high ($\delta > \sim 0.3$, $\beta_p > \sim 2$), the third type of ELM is observed; the wave form is minute-grassy and the edge n_e, T_i and T_e can continuously increase during the grassy ELMs. The behaviors of the three ELMs are similar to those observed in DIII-D [10.2] and have different dependence of f_{ELM} on P_{net}. With increasing P_{net}, dithering ELM appears, $f_{ELM\text{-dither}}$ decreases quickly, then giant ELM appears and $f_{ELM\text{-}giant}$ increases almost linearly with P_{net} [10.3]. With decreasing $B_t^2/(Rq_{eff}^2)$, decreasing l_i or increasing n_e, $f_{ELM\text{-}giant}$ increases. The minute-grassy ELMs have higher f_{ELM} than giant ELMs and no clear dependence on P_{net} has been observed.

10.2 Effects of plasma shape on the onset conditions of the giant ELMs

In JT-60U, an ELM-free phase appears only when $\bar{n}_e$ is lower than a threshold value $\bar{n}_e^{th}$, which increases with I_p or $B_t^2/(Rq_{eff}^2)$ (a measure for the ballooning stability) [10.3]. Since edge n_e and edge T_i & T_e are roughly proportional in JT-60U, the onset condition of the giant ELM is given by a function of edge n_e or edge pressure. The values of $\bar{n}_e^{th}$ are $\sim 1 \times 10^{19} m^{-3}$ at

I_p=1MA and ~3-4x10^{19}m^{-3} at 4MA. To obtain high plasma performance at higher n_e we studied the effects of plasma shape. Recently a new connection of poloidal field coils (now limited at I_p<1.2MA) enabled us to scan triangularity δ from the original value of ~0.1 to δ~0.4 and also down to a negative δ~ -0.06. Figures 10.1 a)-c) compare the typical shapes at I_p=1MA and d) indicates the operation region of δ and elongation κ for the ELM study: the δ-scan at fixed κ, the κ-scan at fixed δ and negative δ.

Figure 10.2 shows the results at I_p=1MA with (δ, κ) ~ (-0.05, 1.55), (0.08, 1.6) and (0.33, 1.4). In Figs. 10.2 a) and b), higher δ has higher $\bar{n}_e$ at the first giant ELM. In addition, the ELM free period (from H-transition to the first giant ELM) was increased from ~0.05 sec to 0.9 sec. (Note: The length of ELM-free period is a rough measure of improvement, because the length is a function of n_e-rise affected by NB power, recycling, etc.) Figures 10.2 (c) and (d) show that edge $\bar{n}_e$ and edge temperatures at the onset of the giant ELMs increase with δ and their improvement from δ~0.08 to δ~0.33 are 30-40% ($\bar{n}_e$) and ~80% (T_e(95%) and T_i(95%)). The edge pressure limit (nXT) increases roughly linearly with δ.

The onset condition of giant ELMs is given by a clear proportionality grad-p^{th}_{edge} ~ $B_t^2/(Rq_{eff}^2)$ over wide ranges of I_p (0.4-4MA) and B_t (1-4T) (Fig. 10.3(b)), where p^{th}_{edge} is a measure of thermal pressure given by $\bar{n}_e$(~0.7a)x(fT_i(95%)+T_e(95%)) and f is a function of Z_{eff}. The pressure gradient parameter grad-p^{th}_{edge} is given by p^{th}_{edge}/ (T_i(95%)$^{0.5}$/B_p(a)). Here we assume the width of the edge pressure pedestal is proportional to the poloidal gyro radius of thermal ions ρ_i ~T_i(95%)$^{0.5}$/B_p(a) based on experiment [10.4]. The normalized pressure gradient α=(grad-p^{th}_{edge})/($B_t^2/(Rq_{eff}^2)$) (tangent in Fig. 10.3(b); proportional to the α parameter used in the high-n ballooning analyses) is almost constant over a wide range of q_{eff}=3-10 at low-δ (Fig. 10.3(c) open circles). This result suggests the giant ELM is triggered by high-n ballooning mode. A time dependent analysis including bootstrap current supports this result [10.5]. Whereas, high-δ plasmas (closed circles) have higher values of α. In Fig. 10.4(a), the α-parameter increases with δ, which is clear for the δ-scan at fixed κ (closed circle). This tendency may saturate around δ~0, because data with δ~0.08 and -0.05 at κ~1.5 have similar values of α (see Figs. 10.4(a) and 10.5(a)). Another important result is that the β_N value at the onset of giant ELM increases with δ (Fig. 10.4(b)). In JT-60U H-mode at δ~0.1, β_N was lower than 1.8 because of giant ELMs [10.1]. The results obtained here shows that the H-mode performance in JT-60U is increasing with δ. Figure 10.5(a) shows the α-value also tends to increase with κ (κ=1.5-1.8) (open circles: δ ~0.1). Finally, at the fixed κ (=1.5-1.6) and δ (=0.06-0.13) the α-value increases with l_i (Fig. 10.5(b)), which indicates the giant ELMs in this (κ,δ) region is related to the high-n ballooning mode in the first stability region.

We simply assumed the width of the edge pedestal is proportional to ρ_i, which should be studied in detail. The width for the high δ and low δ plasmas measured so far seems almost the same at a given B_p(a). Another issue is the contribution of the fast ion pressure gradient. For the

effects of current profile, the region of l_i in the high δ (>0.3) cases in Fig. 10.4 is 0.8-1.6 and almost in the same range of low-δ cases. The study on edge shear at high-δ is our future work including the access to the second stability regime.

10.3 Conclusion

For the standard shape of JT-60U at low triangularity δ (~0.1), onset condition of the giant ELMs is clearly correlated with the high-n ballooning limit in the first stability regime over wide ranges of plasma parameters (I_p, B_t, q_{eff}..). The edge pressure limit increases with elongation κ (1.5-1.8) and internal inductance l_i. The δ-scan (-0.05 ~ 0.4) showed that the limit of edge density, edge pressure and edge pressure gradient increases with δ.

Acknowledgement. The authors gratefully acknowledge contribution by Dr. T. S. Taylor to establish the high triangularity shape in JT-60U.

References

[10.1] Y.Kamada *et al.*, in Plasma Phys. Cont. Nucl. Fusion Res. Proc.15th Int. Conf., Seville, 1994, IAEA-CN-60/A-5-I-5, see also Y. Kamada et al., Nucl. Fusion **34** (1994) 1605 .

[10.2] E. J. Doyle *et al.*, Phys. Fluids **B 3** (1991) 2300.

[10.3] Y. Kamada *et al.*, Plasma Phys. Cont. Fusion **36** Suppl (7) A (1994) A123.

[10.4] M. Kikuchi *et al.*, Proc. 20th Europ. Conf. on Cont. Fusion and Plasma Phys. (Lisboa , 1993) Part I (Geneva:EPS), p. 179.

[10.5] M. Sato *et al.*, in Plasma Phys. Cont. Nucl. Fusion Res. Proc.15th Int. Conf., Seville, 1994, IAEA-CN-60/A2-II-4.
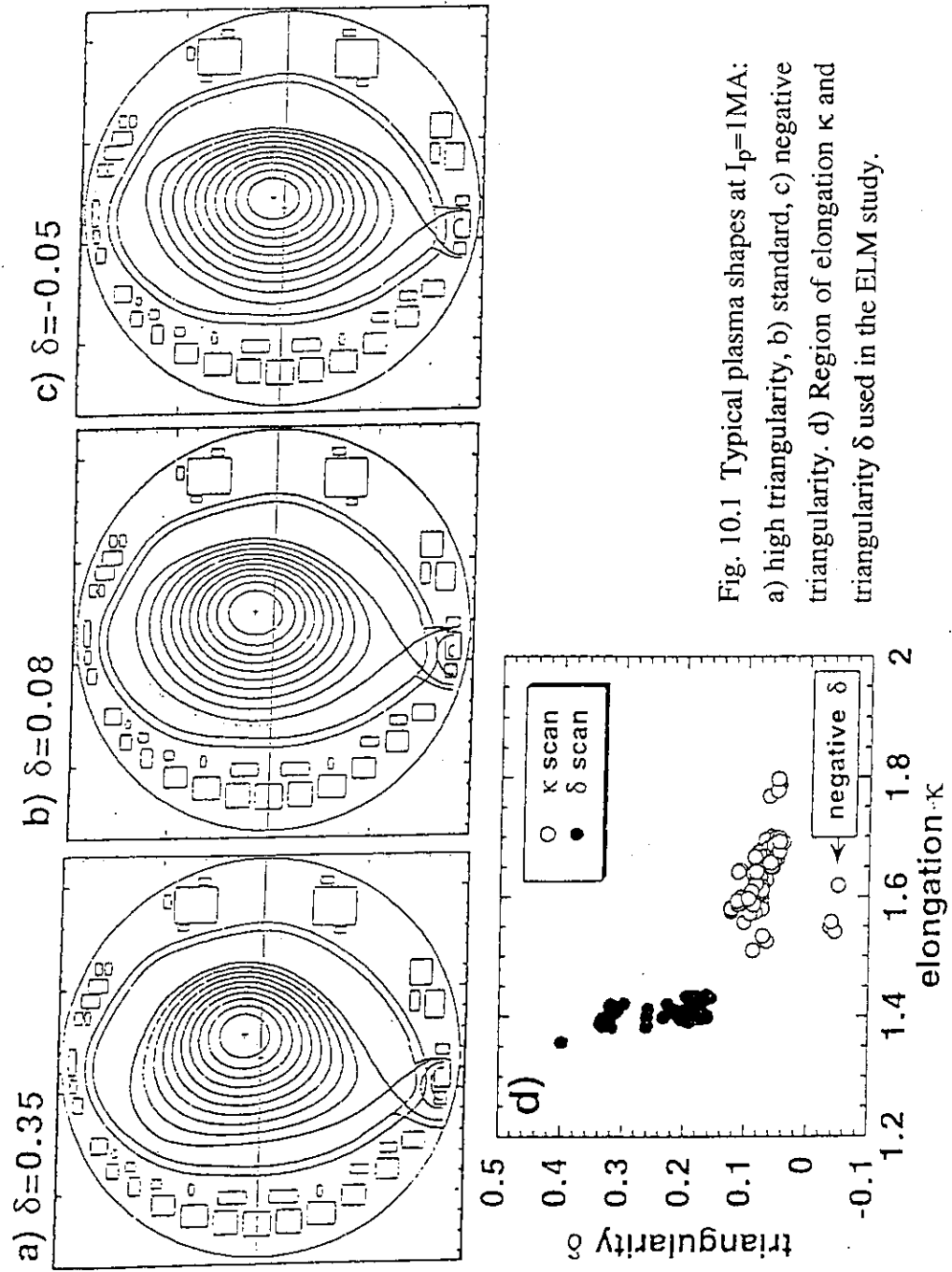
Fig. 10.1 Typical plasma shapes at I_p=1MA: a) high triangularity, b) standard, c) negative triangularity. d) Region of elongation κ and triangularity δ used in the ELM study.

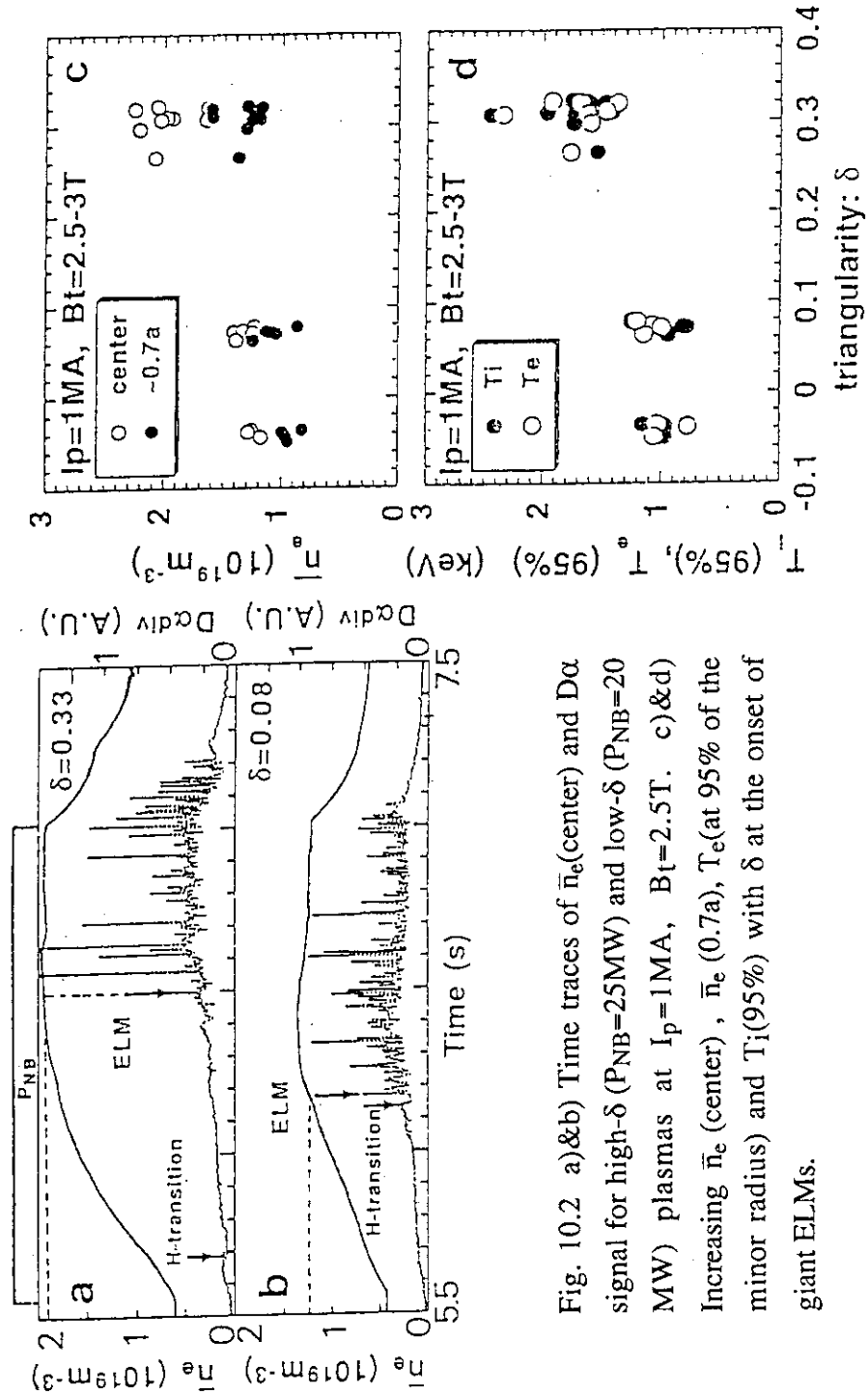Fig. 10.2 a)&b) Time traces of $\overline{n}_e$(center) and $D\alpha$ signal for high-δ (P_{NB}=25MW) and low-δ (P_{NB}=20 MW) plasmas at I_p=1MA, B_t=2.5T. c)&d) Increasing $\overline{n}_e$ (center), $\overline{n}_e$ (0.7a), T_e(at 95% of the minor radius) and T_i(95%) with δ at the onset of giant ELMs.
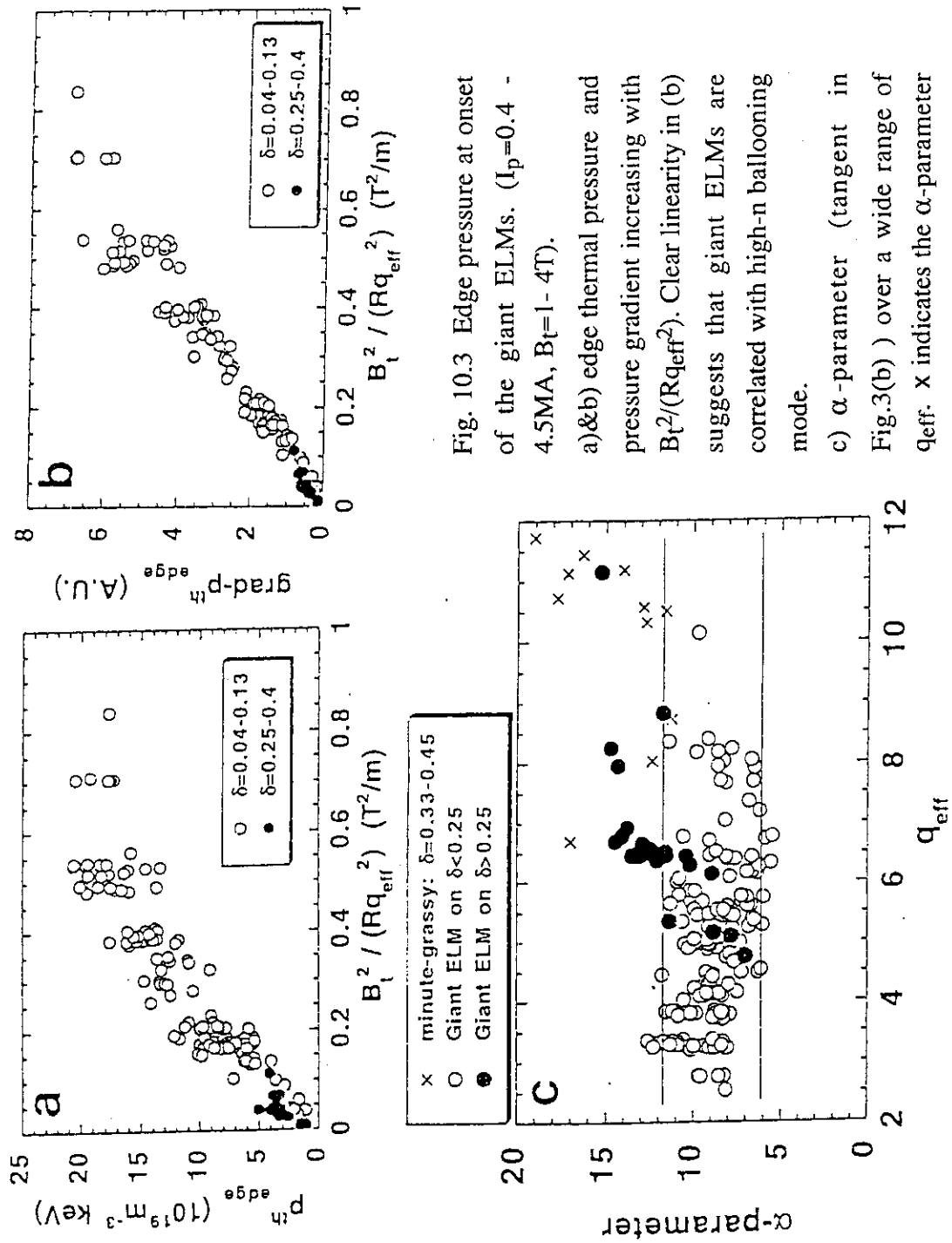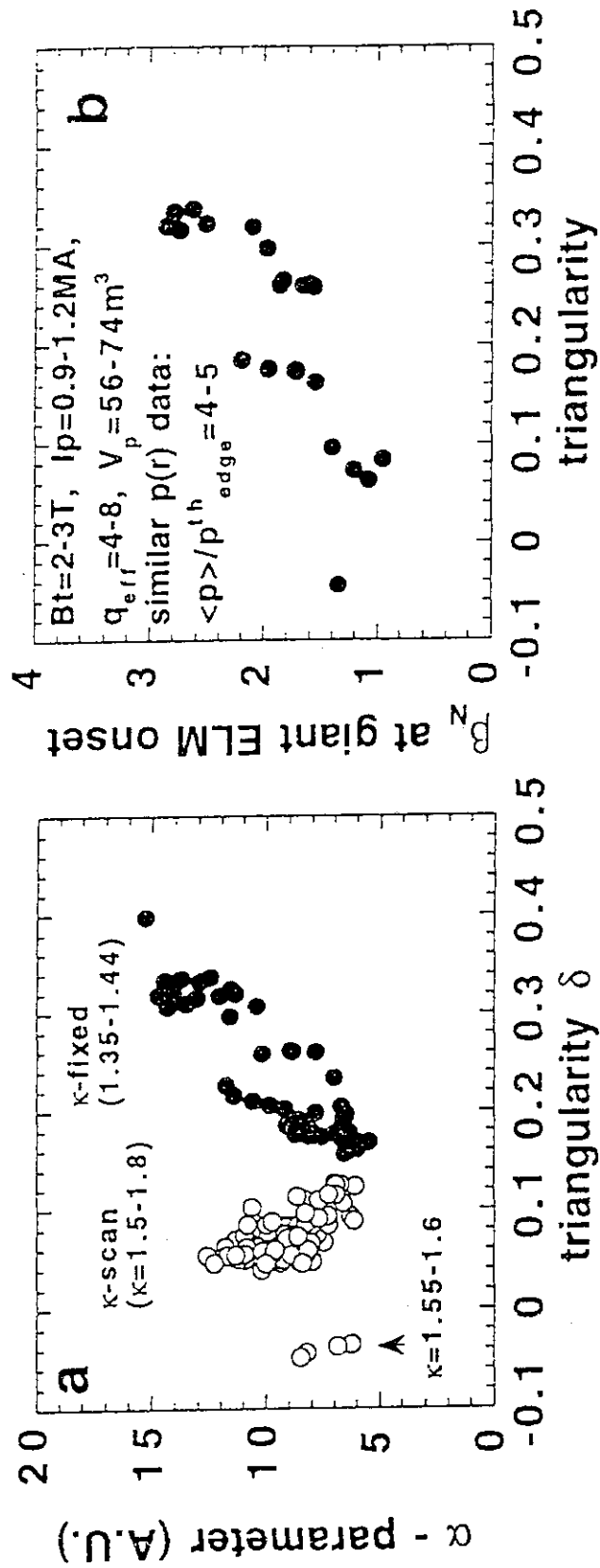
Fig. 10.3 Edge pressure at onset of the giant ELMs. (I_p=0.4 - 4.5MA, B_t=1- 4T).

a)&b) edge thermal pressure and pressure gradient increasing with $B_t^2/(Rq_{eff}^2)$. Clear linearity in (b) suggests that giant ELMs are correlated with high-n ballooning mode.

c) α-parameter (tangent in Fig.3(b)) over a wide range of q_{eff}. x indicates the α-parameter during minute grassy ELMs.

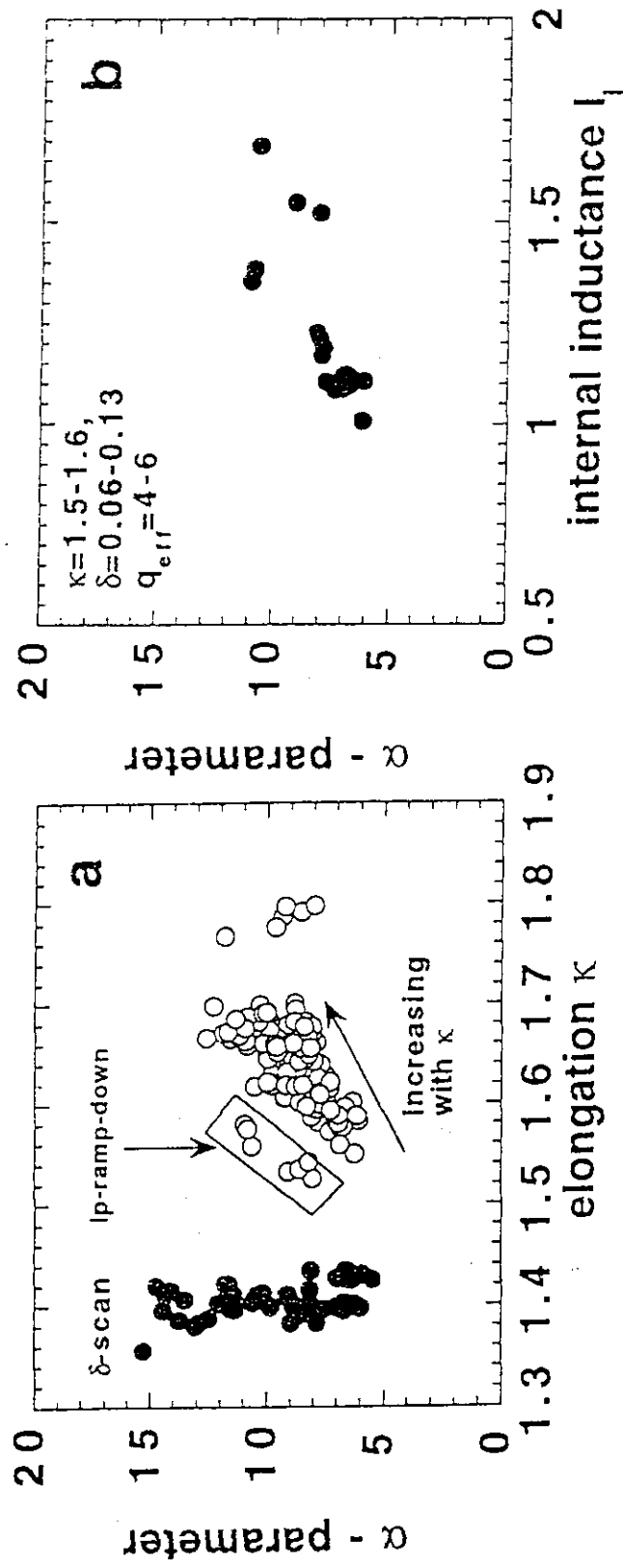Fig. 10.4 Dependence of α-parameter and β_N on triangularity at onset of giant ELMs

Fig. 10.5　Dependence of α-parameter on elongation and l$_i$ at onset of giant ELMs